CHAPTER 4

RESULTS AND DISCUSSION

4.1 Characterisation of palm stearin

4.1.1 Properties of palm stearin

Several characteristics of palm stearin used in this work are summarised in Table 4.1. Palm stearin appears as milky white semi solid at room temperature and it melts into yellow liquid, when heated to temperature above its melting point (45-52 °C). Compared to other drying oils, palm stearin exhibits relatively high melting point and this could due to the close packing of its triglyceride molecules, as majority of the fatty acid chains are composed of saturated hydrocarbons. The composition of palm stearin is given in Table 4.2. Palm stearin is mainly composed of the saturated palmitic acid while the unsaturated acids only make up about 35 % of the total fatty acids composition in the oil. Analysis on iodine value of the palm stearin used in this work shows that the oil has iodine value of 34.2 cg I_2/g oil, and is in good agreement with the literature value of 32-40 cg I_2/g oil (Ghaim & Volz, 2001).

In acid value analysis, the palm stearin used in this work recorded an acid value of 1 mg KOH/g oil. The low acid value, together with high non-volatile content (99.5 %) indicate the oil is well kept and does not experience any significant aging prior to usage.

Table 4.1: Properties of palm stearin

Properties	Results
Appearance	Milky white, semi solid (at room temperature)
	Yellow liquid (> 45 °C)
Acid value / (mg KOH g^{-1} oil)	1.0
Iodine value / (cg I_2 g^{-1} oil)	34.2
Non-volatile content / %	99.5

Table 4.2: Type of fatty acids in palm stearin with its proportions

Fatty acid	Mean/ %	Range/ %
Lauric	0.2	0.1 to 0.3
Myristic	1.4	1.1 to 1.7
Palmitic	59.0	49.8 to 68.1
Palmitoleic	0.5	<0.5 to 1.0
Stearic	4.8	3.9 to 5.6
Oleic	27.4	20.4 to 34.4
Linoleic	7.0	5.0 to 8.9
Lenoleic	0.3	0.1 to 0.5
Arachidic	0.5	0.3 to 0.6
*Total Saturated – 65 %		*Total unsaturated – 35 %

Sources: *Pocketbook of Palm Oil Uses, Fifth Edition* September 2000, Malaysian Palm Oil Board, T.P. Pantzaris, editor Kuala Lumpur, Malaysia

4.1.2 FTIR spectroscopy

FTIR spectrum of palm stearin is shown in Figure 4.1. The spectrum agrees with the general structure of a triglyceride in which the absorption bands of the hydrocarbon chains of fatty acids are observed at 2924 cm^{-1}, 2854 cm^{-1} (C-H stretching of $–CH_3$ and $–CH_2$ groups), 1465 cm^{-1} (C-H bending of $–CH_2$ group), 1377 cm^{-1} (C-H bending of $–CH_3$ group) and 721 cm^{-1} ($-CH_2$ rocking). Peaks at 1746 cm^{-1} (C=O stretching of ester group), 1162 cm^{-1} and 1116 cm^{-1} (C-O stretching of ester) represent the ester linkages in palm stearin.

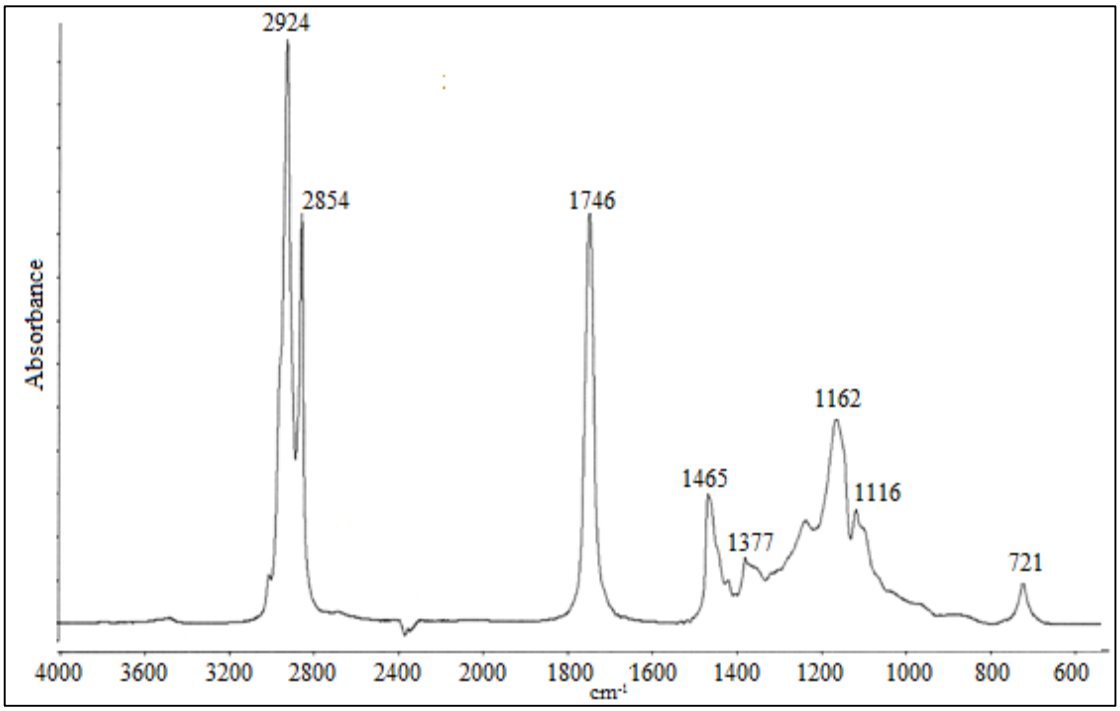

Figure 4.1: FTIR spectrum of palm stearin

4.1.3 ^{1}H-NMR spectroscopy

^{1}H-NMR spectrum of palm stearin is given in Figure 4.2 and the assignment of the various peaks present in the spectrum is shown in Table 4.3. Peaks at 0.8 and 1.3 ppm represent the methyl and methylene protons from the hydrocarbon chain of fatty acids. Presence of unsaturated fatty acids such as oleic acid and linolenic acid in palm stearin are reflected from the resonance of the allylic and vinylic protons at 2.0 and 5.3 ppm respectively. Besides, a weak peak is also observed at 2.7 ppm and it is due to the resonance of protons that are sandwiched between two -C=C- groups, -C=C-C***H₂***-C=C, which mainly exist in linoleic acid. Other peaks observed at 2.3 ppm and 4.1-4.3 ppm correspond to the methylene protons that directly attached to the carbon and oxygen atom of the ester unit.

Table 4.3: Peak assignments for^{1}H-NMR spectrum of palm stearin

Chemical shifts / ppm	Proton assignment
0.8	-R-C***H₃***
1.3	-R-C***H₂***-R-
1.6	-OOC-CH_2-C***H₂***-
2.0	-C=C-C***H₂***-
2.3	-OOC-C***H₂***-
2.7	-C=C-C***H₂***-C=C-
4.1-4.3	-COO-C***H₂***-
5.3	-***H***C=C***H***-

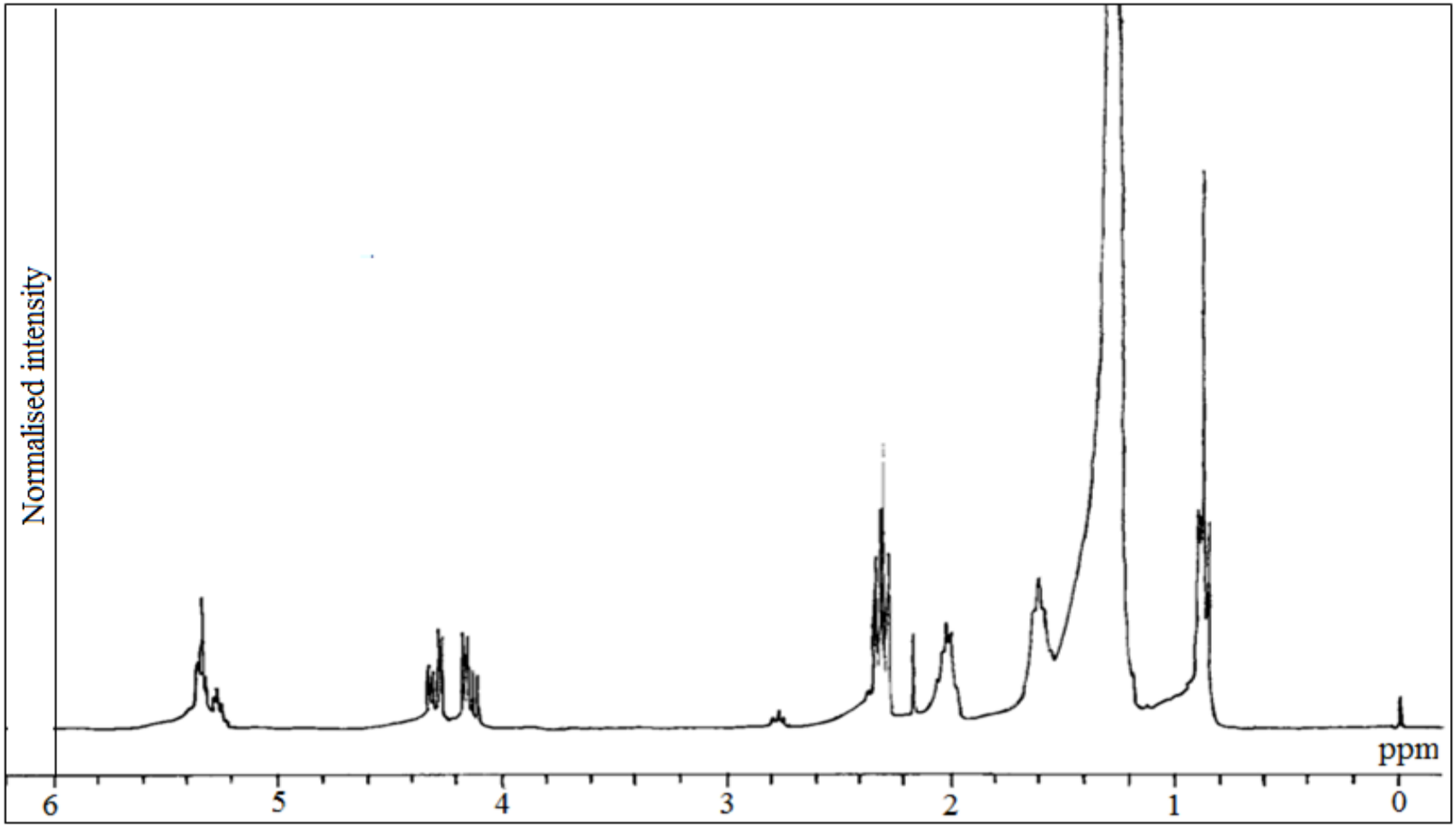

Figure 4.2: ^{1}H-NMR spectrum of palm stearin

4.2 Characterisation of ENR50

4.2.1 FTIR spectroscopy

FTIR spectrum of ENR50 is shown in Figure 4.3. The IR spectrum was obtained after the rubber was masticated for 6 times under room temperature condition. The absorption bands which correspond to the *cis*-1,4 polyisoprene unit in ENR50 are observed at 2860 cm^{-1} (C-H stretching), 1665 cm^{-1} (C=C stretching), 1457 cm^{-1} (C-H bending of $–CH_2$ group), 1375 cm^{-1} (C-H bending of $–CH_3$ group) and 835 cm^{-1} (=C-H out of plane deformation). Other bands at 875 cm^{-1} and 1250 cm^{-1} are attributed to the epoxide groups in ENR50.

Several weak peaks that correspond to secondary reactions involving epoxide groups are observed in the spectrum as well. Among them are the peaks at 1063 and 1110 cm^{-1} which suggests the formation of furanised ring structure and ether links in the rubber. Besides, breakdown of the epoxy ring into secondary alcohol group is confirmed by the absorption bands at 1028 cm^{-1} (-C-O stretching of secondary alcohol group) and 3469 cm^{-1} (R-O-H stretching).

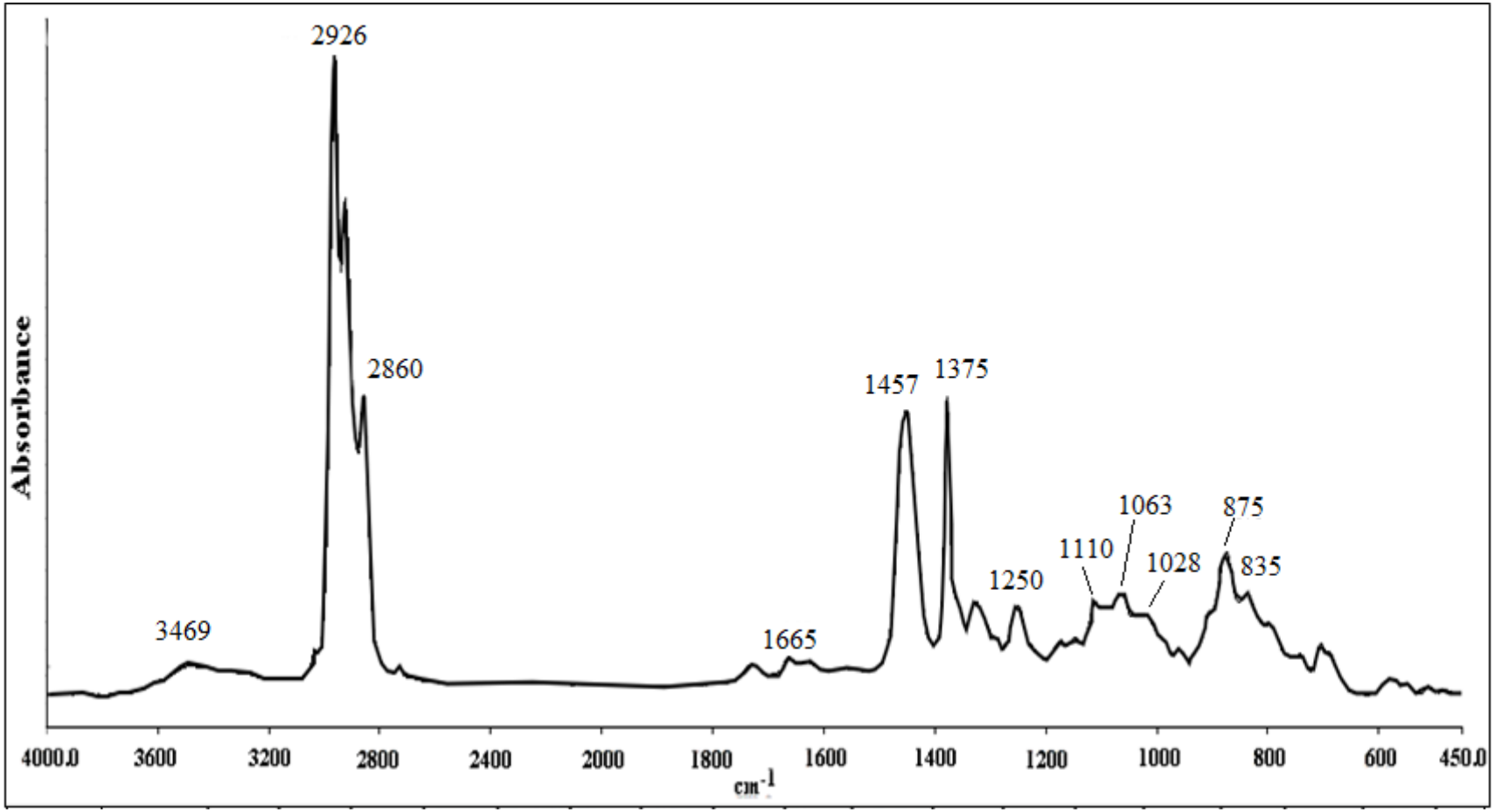

Figure 4.3: FTIR spectrum of ENR50

4.2.2 ^{1}H-NMR analysis

^{1}H-NMR spectrum of ENR50 is given in Figure 4.4 and the assignment of the various peaks present is shown in the spectrum. Three signals characteristic of methyl, methylene and unsaturated methine proton of cis-1,4-isoprene unit are observed at 1.68, 2.05 and 5.1 ppm, respectively. Other signals appeared at 1.29 and 2.7 ppm are assigned to the methyl and methine proton of the oxirane unit, respectively.

The epoxy group content of the rubber used in this work was estimated from the integrated area of the signals at 2.7 and 5.1 ppm, as in Eqn. 3.4. In the equation, the values 1.14 and 1.09 refer to the integrated area of peaks at 2.7 ppm and 5.1 ppm respectively.

$$Epoxy\ content\ of\ ENR\ 50 = \left(\frac{1.14}{1.14 + 1.09}\right) 100\ \%$$

$$= 51.1\ \%$$

$$\approx 50\ \%$$

Based on the calculation, the estimated epoxy group content of ENR50 used in this work is 51.1 %. Therefore, the amount of epoxy groups present in the blend can be calculated by considering ENR50 to consist equimolar amounts of epoxy and isoprene units (50 mol % of epoxide group). The molecular weight of the epoxy and isoprene unit is 84 and 68 g mol^{-1} respectively which adds up to 152 g mol^{-1}. This means in 152 g of ENR50 there is 1 mol of epoxy unit, or in other words there is 6.58 x 10^{-3} mol/g of epoxy groups in ENR50.

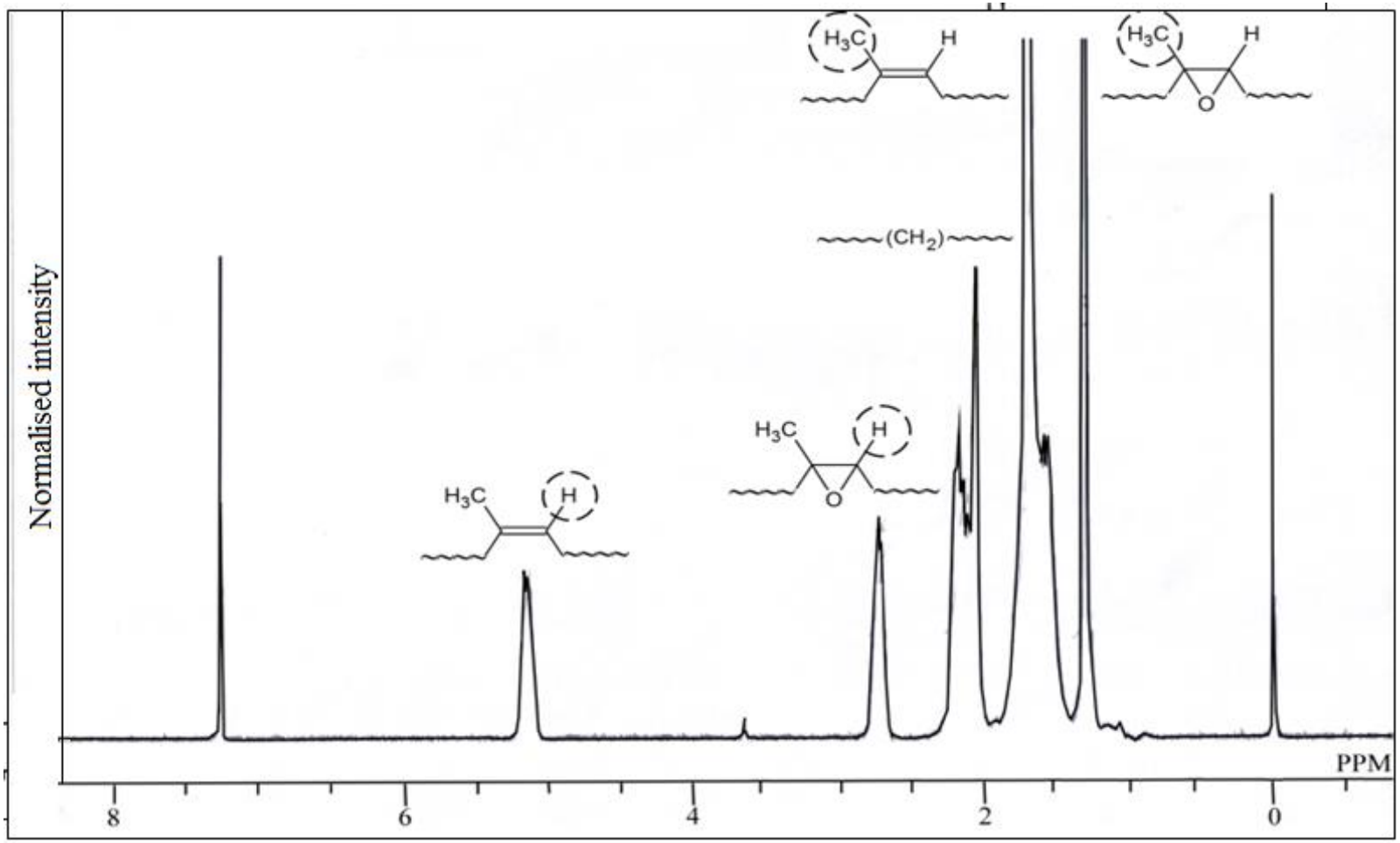

Figure 4.4: [1]H-NMR spectrum of ENR50

4.2.3 DSC analysis

DSC thermogram of ENR50 (Figure 4.5) shows a sharp transition at -19.2 °C, which has been assigned as the T_g of the rubber. T_g of ENR50 is much higher compared to natural rubber (T_g = -72 °C) as the polar nature of epoxy group increases the interchain interaction and subsequently reduced the segmental motion of the main chain in the elastomer (Johnson & Thomas, 2000).

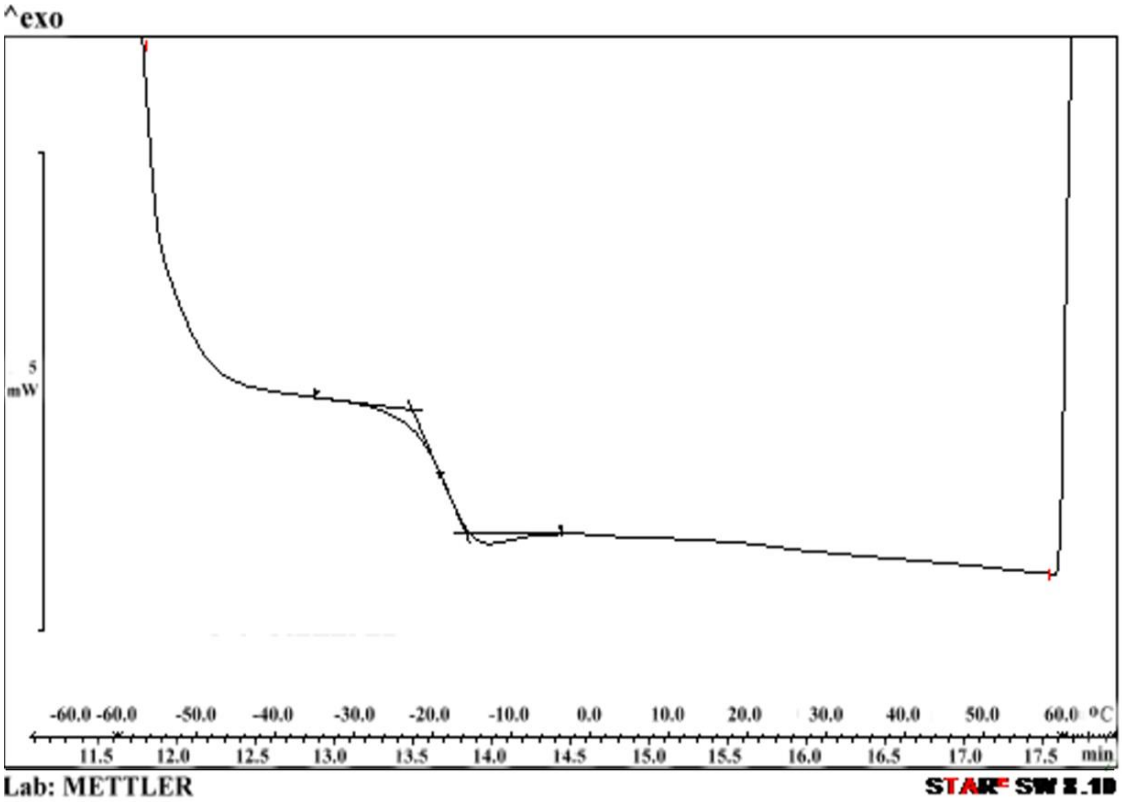

Figure 4.5: DSC thermogram of ENR50

4.3 AlkydCO synthesis

4.3.1 Acid value of reaction mixture during AlkydCO cook

Acid value test were carried out periodically during the esterification process to monitor the progress of AlkydCO cook. Figure 4.6 shows the changes in acid value against esterification time during AlkydCO synthesis. The initial acid value (time = 0 minute) was calculated based on the amount of PA introduced into the system as shown in Section 3.4.2 and the subsequent acid values were determined experimentally by sampling reaction mixture from the alkyd cook at every 30 minutes interval.

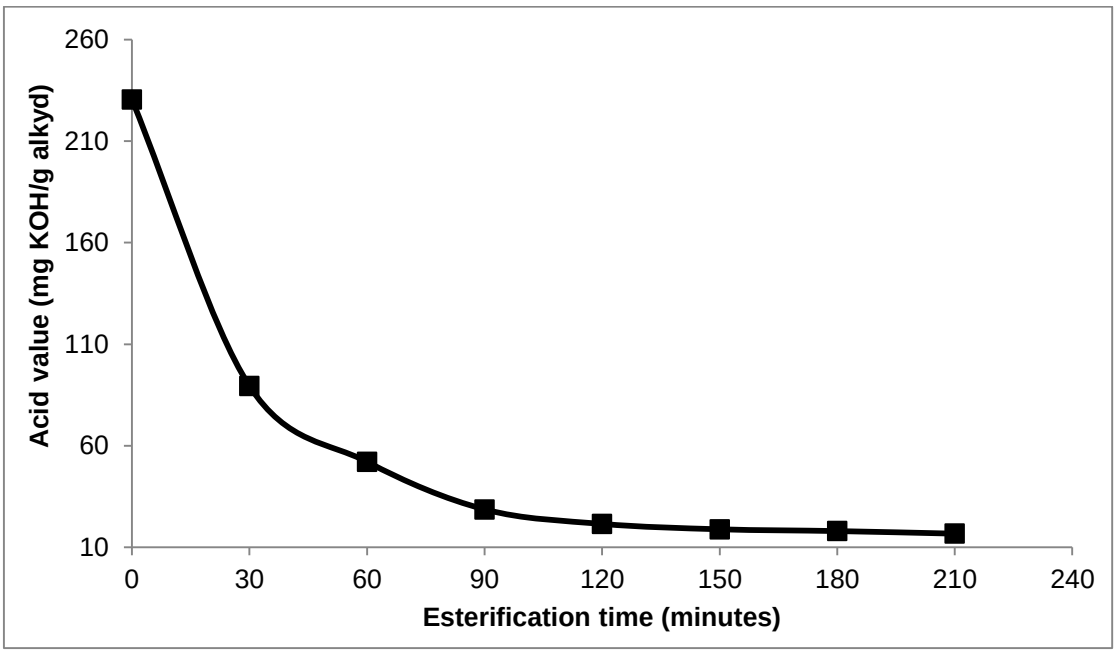

Figure 4.6: Changes in acid value against esterification time during AlkydCO synthesis

Acid value of the reaction mixture decreased as the reaction progressed due to the conversion of the –COOH groups from the incorporated PA into ester linkages. A steep drop in acid value was observed in the early stage of the esterification process, but as the reaction proceeds, the rate of esterification become slower. This is due to the difference in the reactivity of the primary and secondary hydroxyl groups of α-

monoglyceride and glycerol in the alcoholysis products. Since primary hydroxyl group reacts faster than those of secondary, the great decrease in acid value in the early stages of esterification is due to the reaction between PA and the primary hydroxyl groups while the later is due to the reaction with secondary hydroxyl groups (Goldsmith, 1948). Besides, the decrease in the concentration of free acids in the system has lead to the reduction in esterification rate at the end of the reaction (Odetoye et al., 2010). AlkydCO was cooked to the final acid value of 16.7 mg KOH/g alkyd which is also equivalent to 95 % of conversion. The acid value was not reduced further as to avoid the possibility of gelation during the cook.

4.3.2 ^{1}H-NMR spectroscopy of AlkydCO

Figure 4.7 shows the ^{1}H-NMR spectra of palm stearin and AlkydCO. Peaks in the ^{1}H-NMR spectrum of AlkydCO were assigned, and shown in Table 4.4. No significant difference was observed in the region 0-3 ppm between the two spectra as the peaks originated from the resonance of protons from fatty acid chains in palm stearin which were incorporated in AlkydCO chain. However, AlkydCO showed a distinct peak at 3.3 ppm which presumably due to the resonance of proton from –OH groups in the alkyd. This could be possible as AlkydCO was formulated with excess of –OH groups to facilitate the synthesis of modified alkyd with high –COOH content. The presence of significant amount of ester linkages in AlkydCO have resulted in the emergence of broader peaks in the region 3.7-4.1 ppm compared to that of palm stearin. Besides, peaks at 7.5 and 7.7 ppm which correspond to the aromatic protons from the PA unit are observed in the spectrum of AlkydCO.

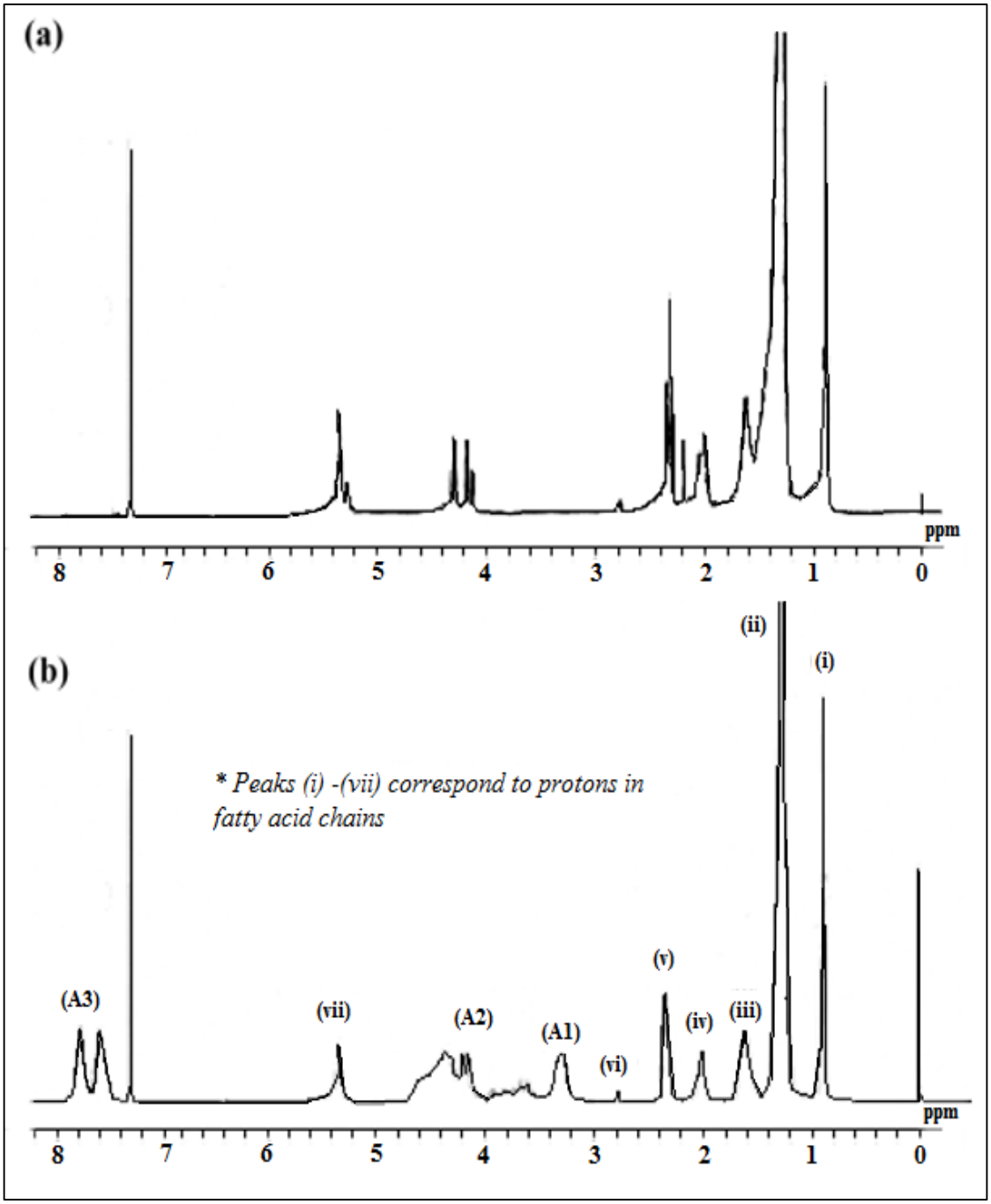

Figure 4.7: ^{1}H-NMR spectra of **(a)** palm stearin and **(b)** AlkydCO

Table 4.4: Peak assignments for ^{1}H-NMR spectrum of AlkydCO

Peaks	Chemical shifts / ppm	Proton assignment
(i)	0.85	-R-C***H₃***
(ii)	1.22	-R-C***H₂***-R-
(iii)	1.57	-OOC-CH_2-C***H₂***-
(iv)	1.97	-C=C-C***H₂***-
(v)	2.30	-OOC-C***H₂***-
(vi)	2.74	-C=C-C***H₂***-C=C-
(A1)	3.32	-CH_2-O***H***
(A2)	3.6 - 4.4	-COO-C***H₂***-, -C***H₂***-OH
(vii)	5.31	-***H***C=C***H***-
(A3)	7.51, 7.69	aromatic –C***H***=C***H***-

Based on the ^{1}H-NMR spectrum, a plausible structure of AlkydCO was derived, and shown in Figure 4.8. It should be mentioned that the structure proposed in the figure is one of the plausible structures, and the two fatty acids shown are randomly picked for ^{1}H-NMR peak assignment purposes and may not represent the dominant species.

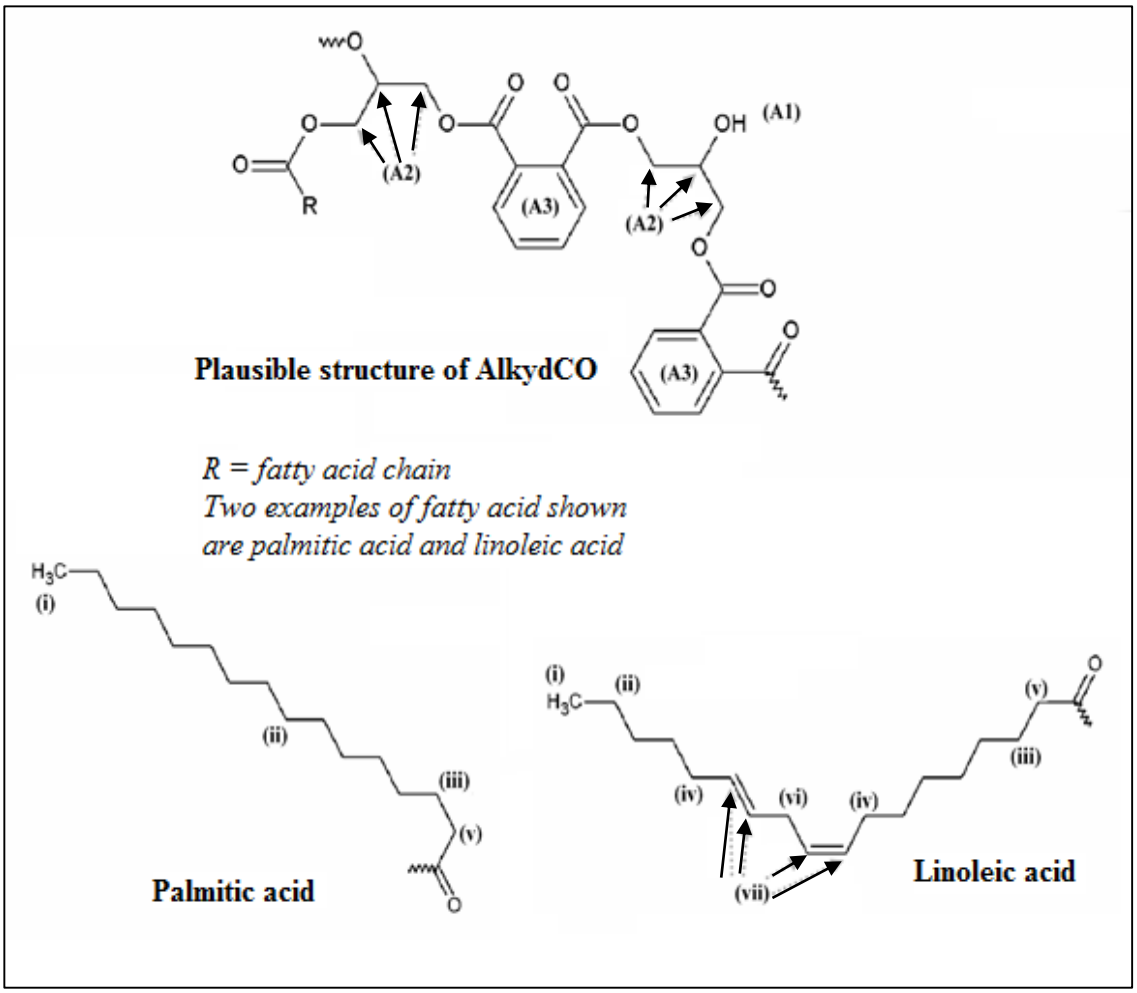

Figure 4.8: Plausible structure of AlkydCO

4.3.3 FTIR spectroscopy of AlkydCO

FTIR spectrum of AlkydCO is shown in Figure 4.9 and the peaks present in the spectrum are assigned in Table 4.5. Comparison on the IR spectrum of AlkydCO with those of palm stearin (Figure 4.1) shows that AlkydCO exhibits additional peaks at 3475 cm^{-1} and 1283 cm^{-1}. During the alcoholysis process, triglycerides in palm stearin were converted to predominant mixture of monoglycerides through reaction with glycerol. This contributes to the high amount of –OH groups present in the system. Subsequently, the –OH groups were consumed in the esterification reaction with the incorporated PA thus generating significant amount of ester linkages as shown by the strong –C-O stretching peak of the ester groups at 1283 cm^{-1}. Despite of the significant consumption

of –OH groups in the esterification process, the –OH stretching at 3475 cm^{-1} in the spectrum was relatively strong as AlkydCO was formulated with stoichiometric excess of –OH groups. The plausible synthesis route of AlkydCO is shown in Figure 4.10.

Table 4.5: FTIR peak assignments of AlkydCO

Wave number (cm^{-1})	Corresponding chemical group	Assignment
743	-C=CH	Aromatic =C-H bending
1071, 1122 & 1283	-COOH	C-O stretching of ester and C-O stretching of carboxyl group
1377	$-CH_3$	C-H bending of $-CH_3$
1457	$-CH_2$	C-H bending of $-CH_2-$
1580 & 1599	-C=CH	Aromatic C=C stretching
1735	C=O	C=O stretching of carboxyl group and C=O stretching of ester
2854	$-CH_2$	C-H stretching of $-CH_2-$
2925	$-CH_3$	C-H stretching of $-CH_3$
3475	-OH	-OH stretching

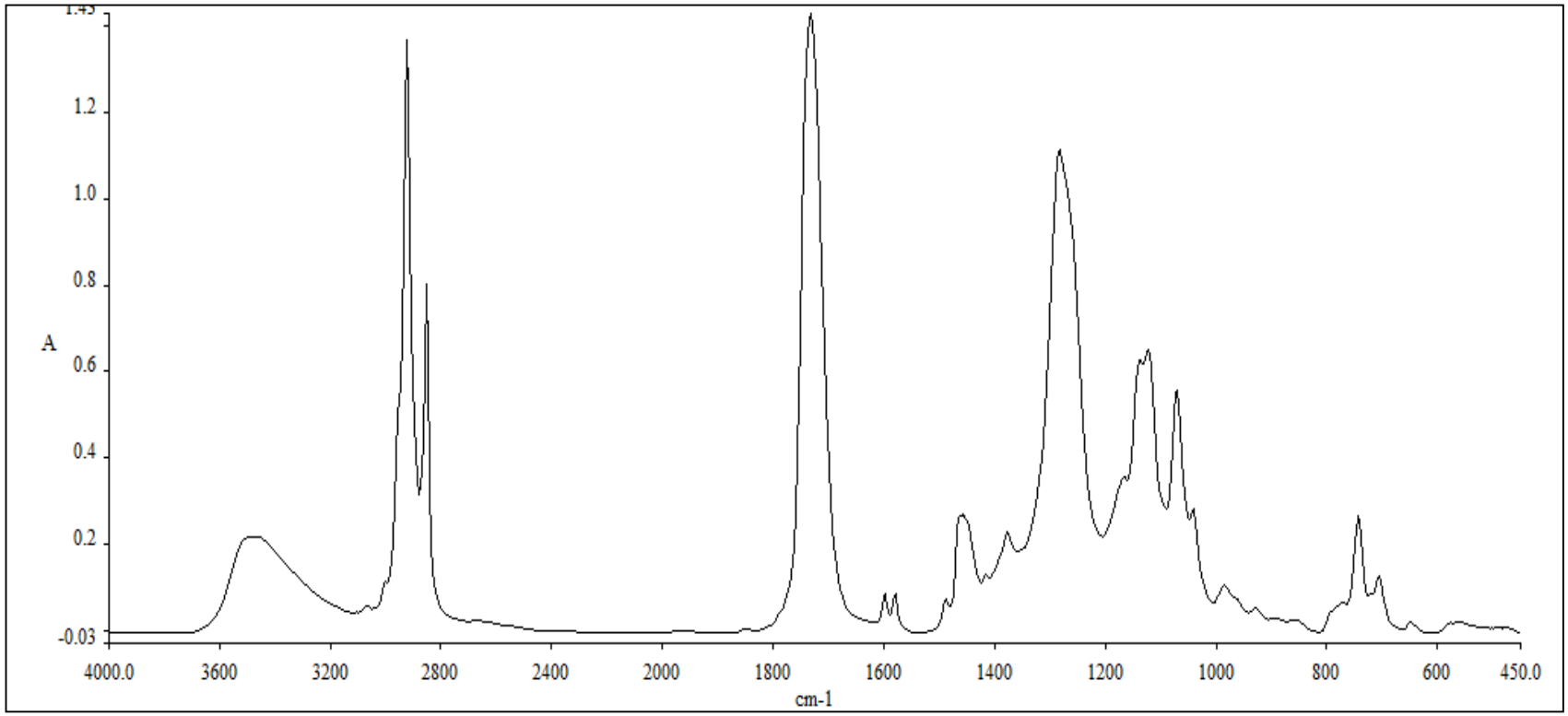

Figure 4.9: FTIR spectrum of AlkydCO

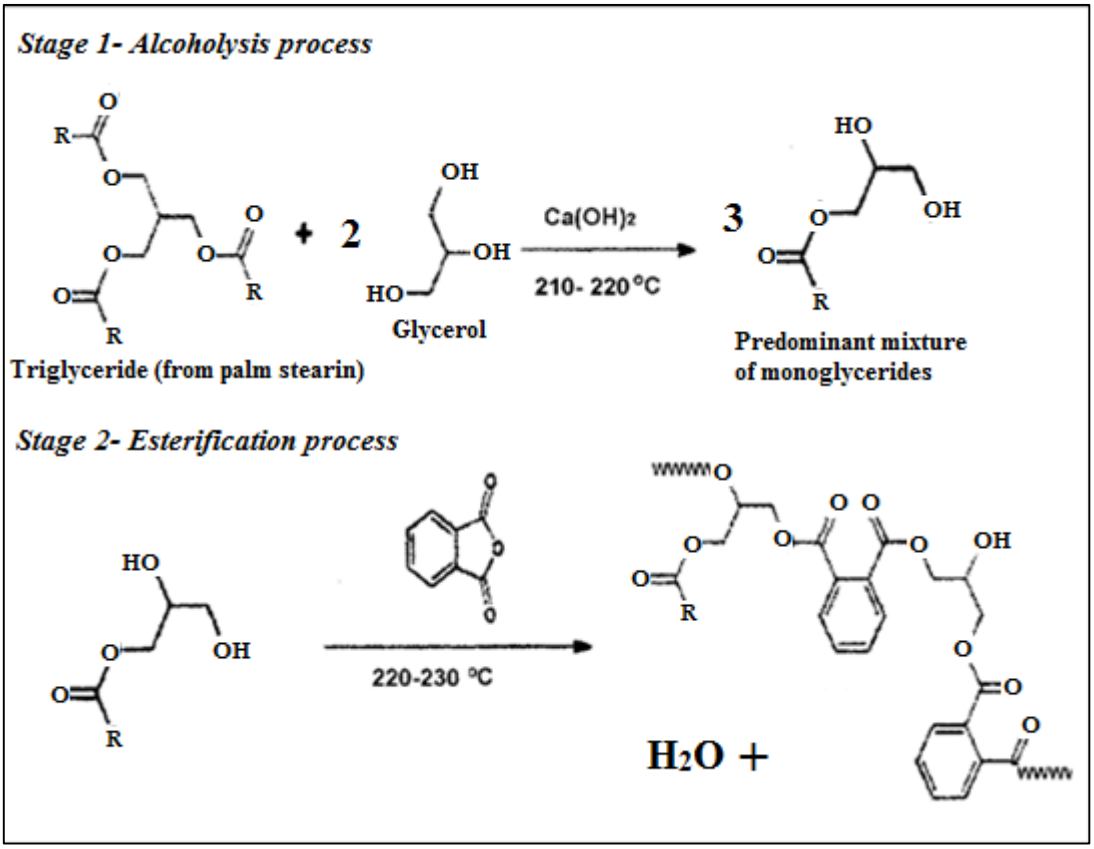

Figure 4.10: Plausible synthesis route of AlkydCO

4.4 Characterisation of alkyds

4.4.1 Final acid value and hydroxyl value of alkyds

Table 4.6 shows the hydroxyl value, initial and final acid values of the alkyds, along with the amount of -COOH groups present. AlkydCO has the lowest amount of –COOH groups in its chain, 3.0 x 10^{-4} mol/g, while AlkydMA1 and AlkydPA1 have slightly more –COOH groups, approximately 8.0 x 10^{-4} mol/g, followed by AlkydMA2 with the highest –COOH content, 12.2 x 10^{-4} mol/g. The increase in the amount of –COOH groups in the modified alkyds is the result of incorporating anhydrides into AlkydCO. Under controlled reaction temperature, the anhydrides were ring-opened in its reaction with –OH groups that are present along the AlkydCO chain, which resulted in the formation of half ester, with –COOH groups grafted as pendant chains in the alkyd.

The plausible synthesis route for the modified alkyds is shown in Figure 4.11. The experimental observation agrees with the proposed route as there is no water evolved during the reaction. Similar results were reported by Ataei et al. (2011) where ring opening of the incorporated anhydride to form half ester results in decrease in acid value, without formation of water. In addition, reduction in the hydroxyl value from 148.5 mg KOH/g alkyd in AlkydCO to 118.0, 120.1 and 80.8 mg KOH/g alkyd in the modified alkyds confirms the participation of –OH groups in the half-ester formation with the incorporated anhydrides.

Two safety measures were taken during the synthesis of modified alkyds with the purpose of preserving the amount of –COOH groups generated. The first measure was maintaining a lower reaction temperature during the incorporation of anhydrides, 120-130 °C (for AlkydMA1 and AlkydMA2) and 160-170 °C (for AlkydPA1). Generally, higher temperature will results in undesirable polyesterification between the free –COOH and –OH groups in the alkyd (Khong & Gan, 2013). Besides temperature control, the alkyd cook was stopped when the acid value of the modified alkyd has dropped to half of the value after all the anhydride has been loaded into the system. This could prevent the newly generated –COOH groups from participating in the esterification as well.

Table 4.6: Hydroxyl value, initial acid value, final acid value, and amount of -COOH groups of alkyds

Alkyd	Hydroxyl value[a] /mg KOH g^{-1} alkyd	Initial acid value[b] /mg KOH g^{-1} alkyd	Final acid value[c] / mg KOH g^{-1} alkyd	Amount of –COOH[d] / 10^{-4} mol g^{-1} alkyd
AlkydCO	148.5	230.5	16.7	3.0
AlkydPA1	118.0	73.5	46.0	8.2
AlkydMA1	120.1	75.0	44.0	7.8
AlkydMA2	80.8	129.3	68.7	12.2

[a]Obtained from hydroxyl value test
[b]Initial acid value = Number of acid equivalents x (56100 / total weight of reactants charged)
[c]Obtained from acid value test
[d]Amount of –COOH = Final acid value/ 56100 mg KOH mol^{-1}

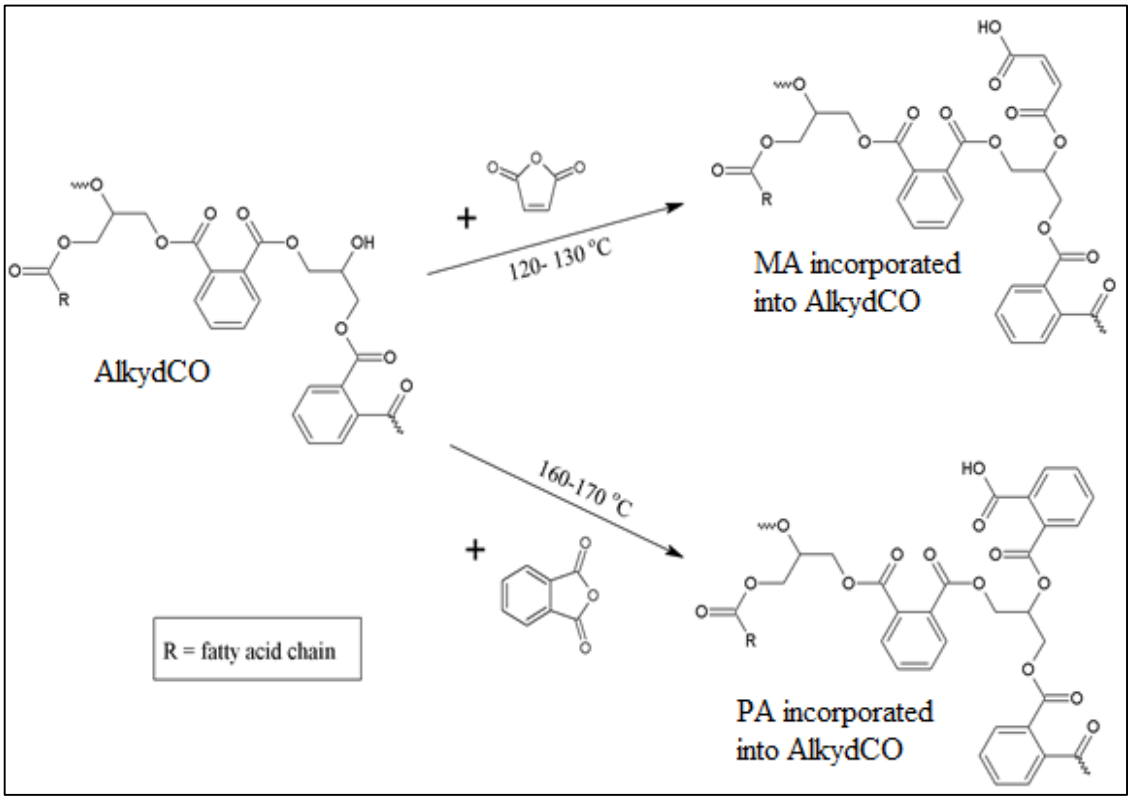

Figure 4.11: Incorporation of anhydrides into AlkydCO

4.4.2 FTIR spectroscopy of alkyds

Figure 4.12 shows the FTIR spectra of all the alkyds synthesised in this work. Qualitatively, the spectra of the alkyds are quite similar with each other as they were synthesised from the same raw materials but with different types of incorporated anhydrides. A weak peak at 1641 cm^{-1} which attributed to the C=C stretching from the incorporated MA can only be observed in the FTIR spectra of AlkydMA1 and AlkydMA2. Besides, stronger –OH stretching peak at 3472 cm^{-1} was observed in the FTIR spectrum of AlkydCO owing to the presence of excess –OH groups in its alkyd chain. The peaks however become weaker in the spectra of all the modified alkyds.

The relative amount of –OH groups in the alkyds were calculated from their FTIR absorbance spectra, and shown in Table 4.7. Peak absorbance at 1457 cm^{-1} which corresponds to C-H bend of $-CH_2$ group was chosen as internal standard to normalise the effect of uneven sample thickness during FTIR scan. The trend in A_{3472}/A_{1457} obtained from the FTIR spectra of the alkyds is in agreement to the hydroxyl value reported in Table 4.6. The decreasing value of A_{3472}/ A_{1457} in the modified alkyds as compared to AlkydCO indicates decreasing amount of –OH groups in the alkyds due to half-ester formation with the incorporated anhydrides.

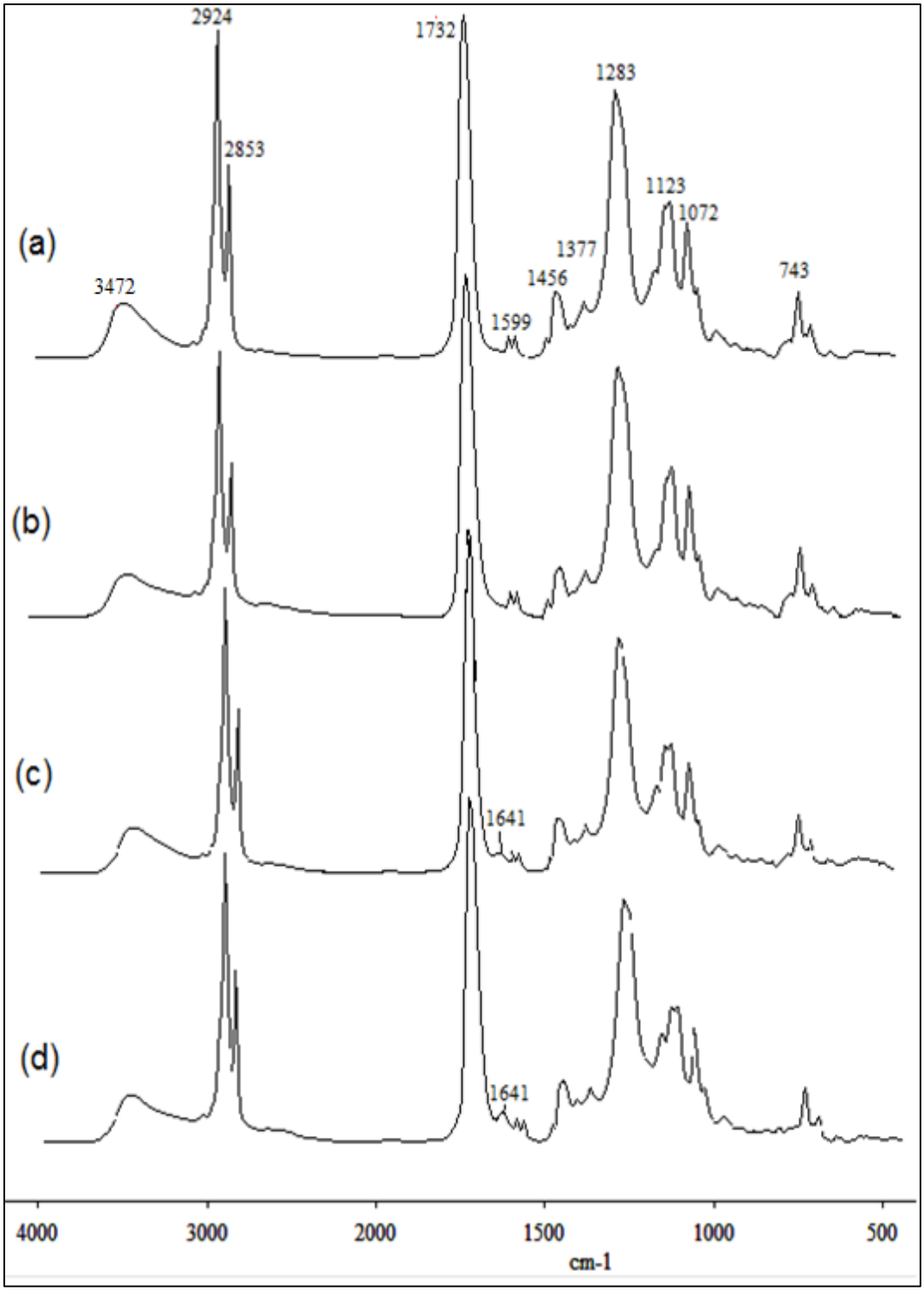

Figure 4.12: FTIR spectra of (a) AlkydCO, (b) AlkydPA1, (c) AlkydMA1, and (d) AlkydMA2

Table 4.7: FTIR peak absorbance at 3472 cm^{-1} (A_{3472}), 1457 cm^{-1} (A_{1457}) and A_{3472} / A_{1457} of alkyds

Alkyd	A_{3472}	A_{1457}	A_{3472} / A_{1457}
AlkydCO	13.1	1.17	11.2
AlkydPA1	6.54	0.68	9.7
AlkydMA1	6.29	0.65	9.7
AlkydMA2	29.4	3.33	8.8

4.4.3 ^{1}H-NMR spectroscopy of alkyds

^{1}H-NMR spectra of AlkydCO, AlkydPA1 and AlkydMA1 are shown in Figure 4.13. A distinct difference between the spectra lies in the region 3.3 ppm where a strong peak which corresponds to the resonance of the hydroxyl proton (-O**H**) was observed in the AlkydCO spectrum. The peak is rather obvious in the ^{1}H-NMR spectrum of AlkydCO as it was formulated with excess of –OH groups. However, the peak is no longer noticeable in the spectra of all the other alkyds, suggesting some of the –OH groups from AlkydCO have reacted with the incorporated anhydrides to form half-ester. The emergence of broader peaks in the region 3.7-4.1 ppm in spectra of the modified alkyds as compared to that of AlkydCO suggests formation of considerable amount of ester linkages resulted from the incorporation of anhydrides.

Besides, an additional peak at 6.3 ppm which attributed to the resonance of vinyl protons from the incorporated MA, -OOC-C***H***=C***H***-COOH was observed in the spectrum of AlkydMA1. The other peaks present in the alkyds spectra are similar to each other as all of them were cooked using similar raw materials. The ^{1}H-NMR spectrum of AlkydMA2 is not included in the discussion as the peaks in the spectrum are similar to those in AlkydMA1 and no noticeable difference was observed throughout the cooking process.

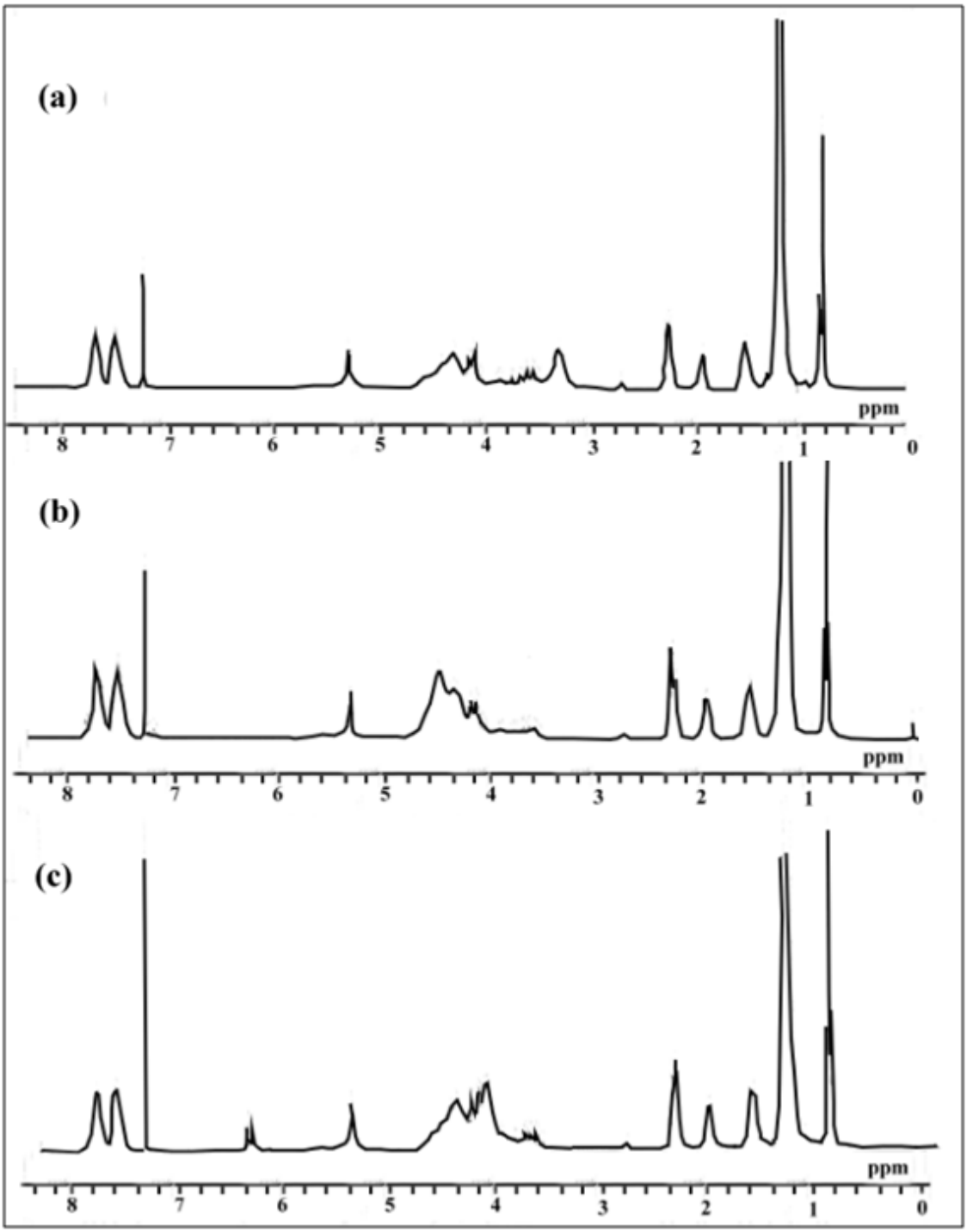

Figure 4.13: ^{1}H-NMR spectra of (a) AlkydCO, (b) AlkydPA1, and (c) AlkydMA1

4.4.4 DSC Analysis

Figure 4.14 shows the DSC thermograms of all the alkyds synthesised in this work. No significant difference was observed in the thermograms of the alkyds as all of them recorded T_g between -21 to -22 °C. Several endothermic peaks were also observed after the T_g of the alkyds. These peaks could be the melting peaks of alkyd. Alkyd is a semicrystalline polymer (Kridli, 2006; Deligny & Tuck, 2000) which appears as semi-solid at temperature below 10 °C but become flowable viscous liquid around 30 °C. In order to confirm the identity of these peaks, a sample of AlkydCO was scanned through repeated heating and cooling and DSC thermogram of the alkyd is shown in Figure 4.15. The endothermic peaks reappear on the second heating cycle, suggesting that these peaks are due to physical transition and most probably is the melting transition of the semi-crystalline alkyd. Multiple melting peaks observed in the temperature range 0-50 °C are attributed to broad distribution of crystallites sizes in the alkyd (Menczel et al., 2009, p. 100).

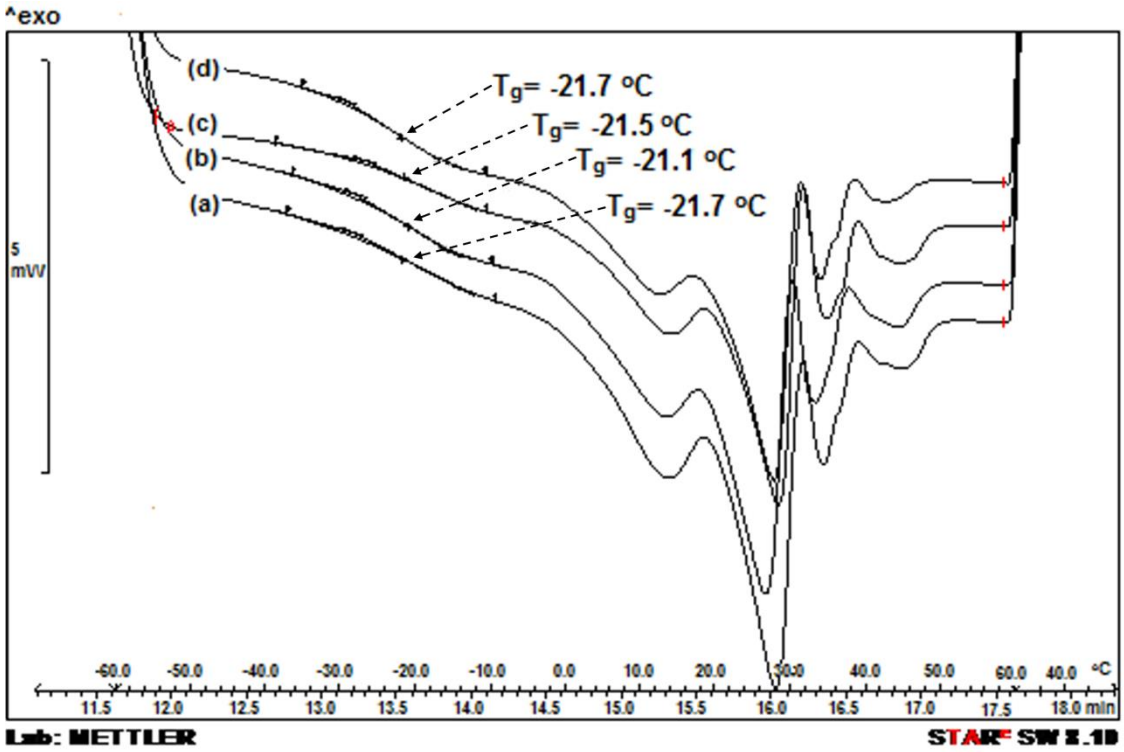

Figure 4.14: DSC thermograms of (a) AlkydCO, (b) AlkydPA1, (c) AlkydMA1, and (d) AlkydMA2

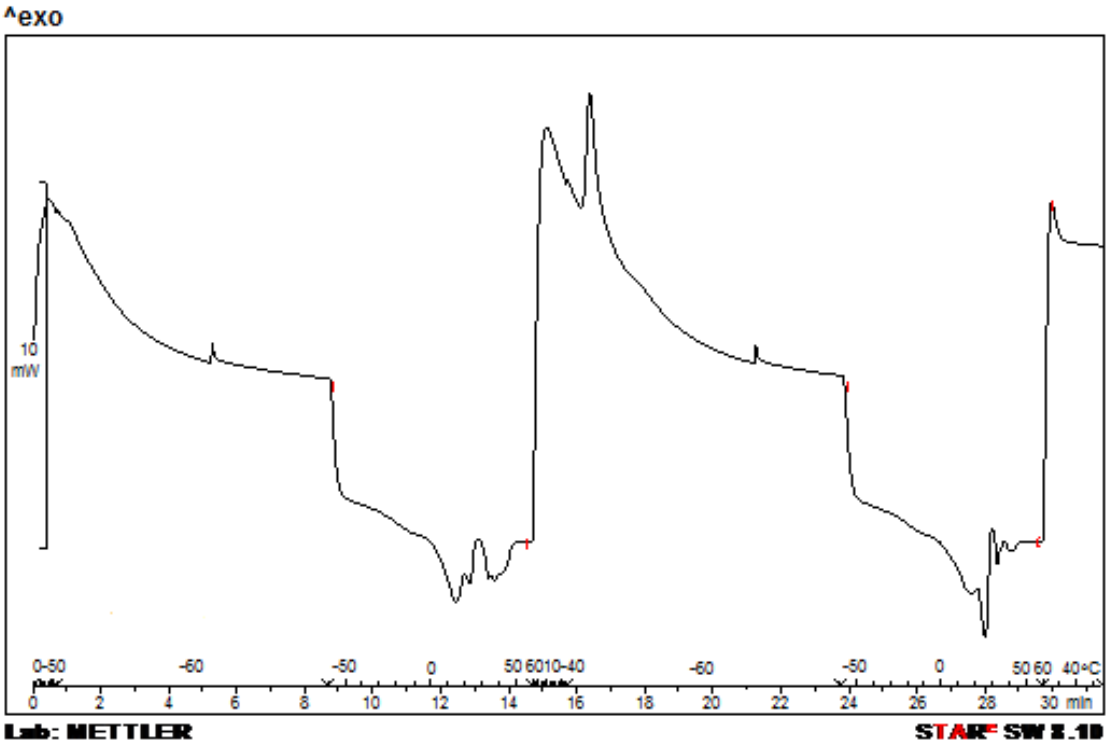

Figure 4.15: DSC thermogram of AlkydCO obtained from repeated heating and cooling

4.5 Characterisation and properties of ENR50/Alkyd blends: Effect of –COOH content in MA-modified alkyds

4.5.1 Reactions during blending

Blending of ENR50 and alkyd was carried out via solvent casting technique using toluene. At the end of specified blending time, the blend solution was coated on glass panel and soaked in methanol in order to precipitate the rubber blend while dissolving the unreacted alkyd. Thin films of the blend were obtained after series of drying process which includes blow-drying in fume hood for 24 hours at room temperature and subsequently drying in vacuum oven at 60 °C. In the work of Gan & Burfield (1989), it was reported that activation energy for the reaction involving ENR50 with benzoic acid in solid form is quite high, approximately 70 kJ mol^{-1}. Such reaction only occurred when ENR50 and benzoic acid were heated at temperature as high as 160 °C. Drying the blend film at 60 °C is expected to accelerate the removal of the trapped solvent only and would not affect the extent of crosslinking that has taken place during solution blending.

Figure 4.16 shows the FTIR spectra of AlkydMA1, ENR50 and ENR50/AlkydMA1 blend (after blended for 12 hours). The spectrum of ENR50/AlkydMA1 blend is similar to ENR50 but with a few additional peaks observed at 3472 cm^{-1}, 1735 cm^{-1} and 1282 cm^{-1}, attributed to the alkyd component in the blend. The peaks present in the spectrum of ENR50/AlkydMA1 blend were assigned, and shown in Table 4.8.

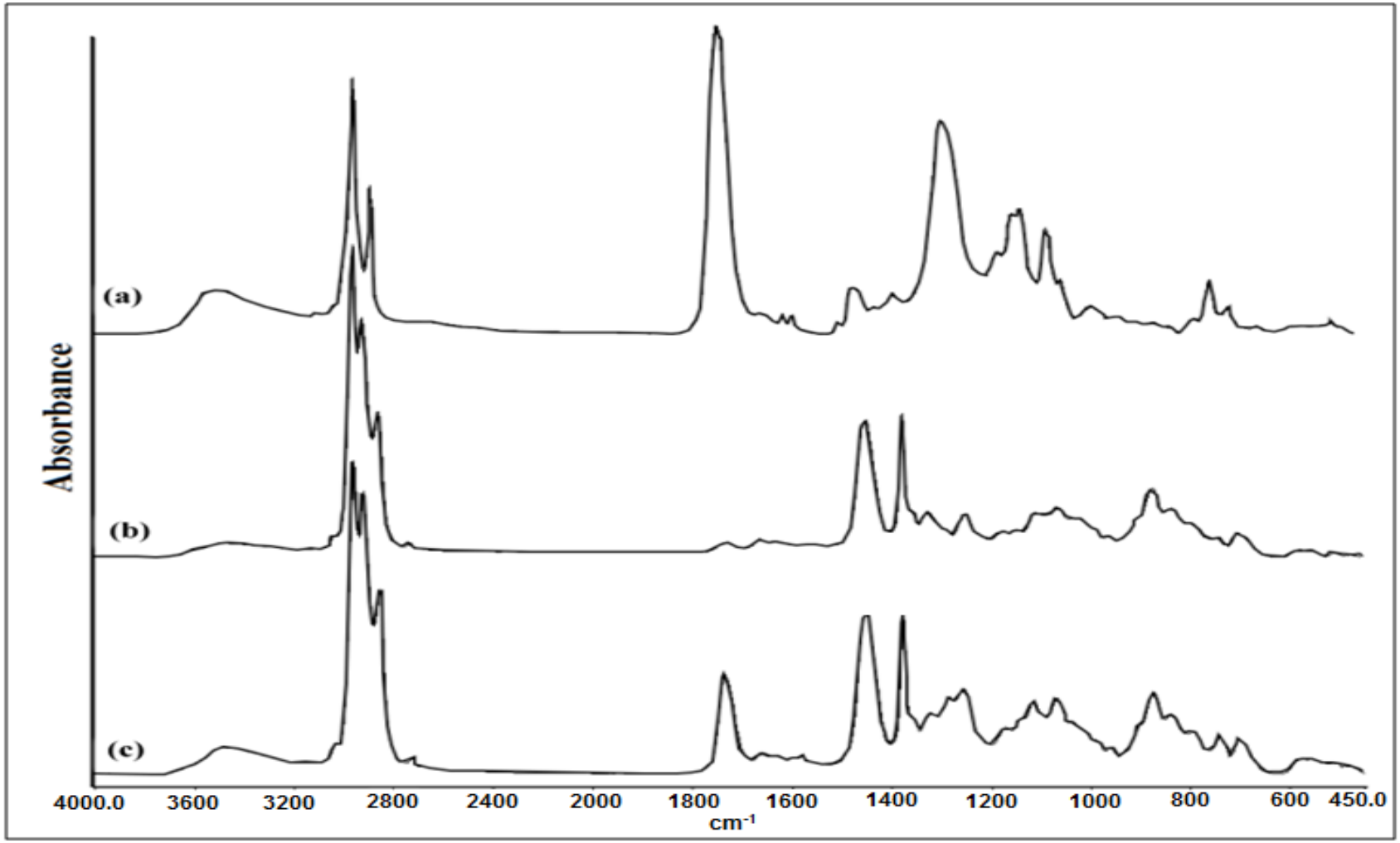

Figure 4.16: FTIR spectra of (a) AlkydMA1, (b) ENR50, and (c) ENR50/AlkydMA1 blend (blended for 12 hours).

Table 4.8: Peak assignments for FTIR spectrum of ENR50/AlkydMA1 blend

Wavenumber (cm^{-1})	Assignment
732	Aromatic =C-H bending
835	=C-H of isoprene unit (out of plane deformation)
875	Epoxy ring vibration
1070, 1116, 1170	C-O stretching (ester, 2° alcohol, ether)
1256, 1282	C-O stretching (carboxylic acid, epoxy ring, ester)
1378	C-H bending (CH_3)
1451	C-H bending (CH_2)
1580, 1599	C=C stretching (aromatic ring)
1662	C=C stretching (isoprene unit, MA unit)
1735	C=O stretching (ester, carboxylic acid)
2858, 2926, 2963	C-H stretching
3490	O-H stretching

ENR50/AlkydMA1 blend series obtained from different blending times were analysed using FTIR to study the changes in the spectrum during blending. Figure 4.17 shows the normalised FTIR spectra of ENR50/AlkydMA1 blend series with different blending time along with the expanded spectra of the blend in the region 870-885 cm^{-1}. The peaks in the spectra were normalised against peak at 835 cm^{-1} to overcome the effect of different sample thickness during FTIR scan.

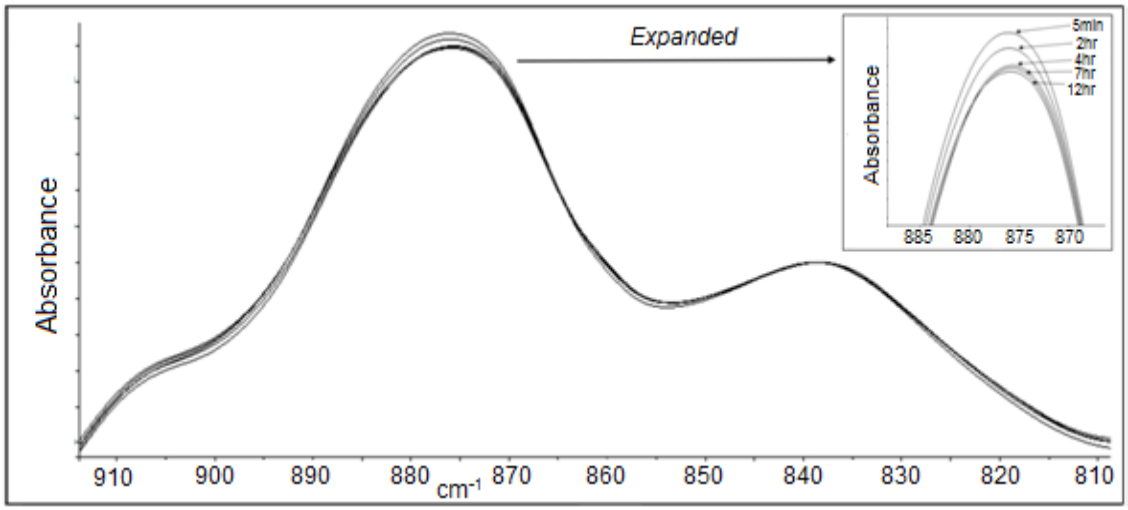

Figure 4.17: Normalised FTIR spectra of ENR50/AlkydMA1 blend series

Based on the figure, the peak absorbance at 875 cm^{-1} which corresponds to the epoxy ring vibration has progressively decreased with blending time, indicating some of the epoxide groups were consumed during the blending (Lee et al., 2011). A steep reduction in the epoxide concentration was observed when the blending time was prolonged from 5 minutes to 4 hours. Further blending however resulted with only small decrease in the epoxide content of the blend. Initially, the concentration of epoxide and -COOH groups were high, leading to the high rate of reaction between ENR50 and alkyd, but as the reaction proceed, the concentration of the reactive groups decreased, and lower rate of reaction is observed. Besides that, formation of crosslink during blending has increased the viscosity of the blend, causing the components in the system become less mobile, and consequently slows down the reaction.

The plausible reaction that took place during solution blending of ENR50 and AlkydMA1 is shown in Figure 4.18. At room temperature (30 °C), epoxide group of ENR50 was ring-opened by the -COOH group from AlkydMA1 to form a hydroxyl group on the rubber chain, and an ester linkage between the rubber and alkyd. Since AlkydMA1 has much lower molecular weight compared to ENR50, formation of an ester linkage would be equivalent to having a small alkyd side-chain grafted onto the

rubber. However, when more than one -COOH groups from an alkyd chain have reacted with more than one epoxide groups from different ENR molecules; effective crosslink was formed in the system.

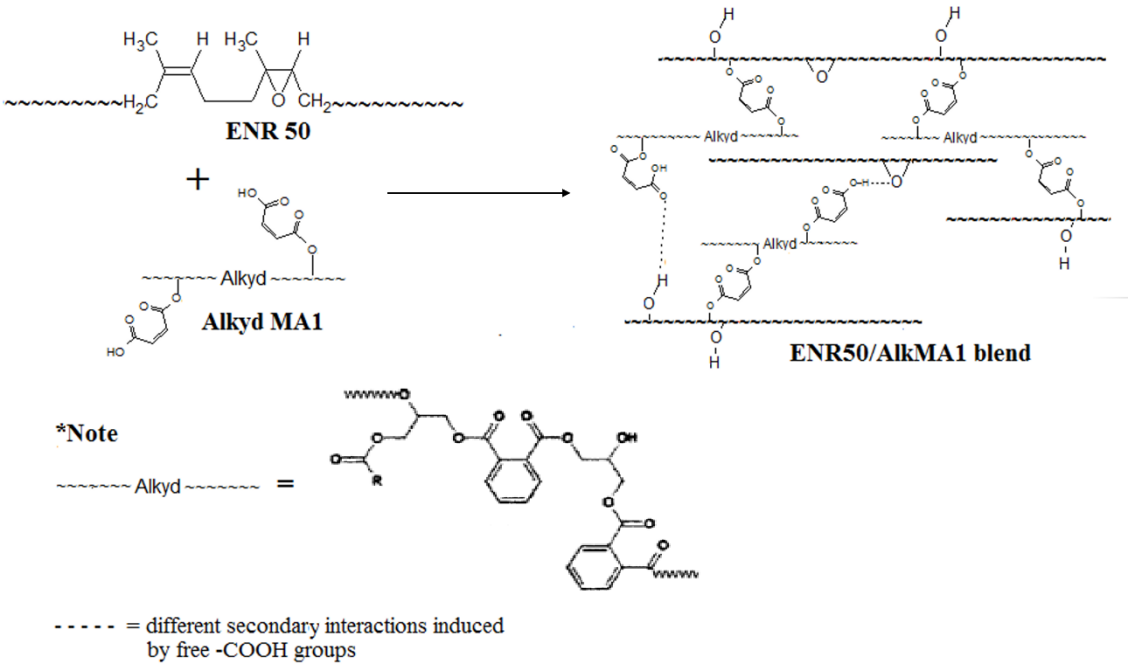

Figure 4.18: Plausible reaction between ENR50 and AlkydMA1 during blending

4.5.2 Comparison between blends from alkyds with different –COOH content (AlkydMA1 and AlkydMA2)

(a) FTIR analysis

The progress of reaction between ENR50 and alkyd with different –COOH content is reflected by the changes in the peak absorbance of the epoxide group at 875 cm^{-1}, normalised to an internal standard peak at 835 cm^{-1}, A_{875}/A_{835}. The epoxide content in each blend that was mixed for 5 minutes were compared to those blended for 12 hours, and the results are tabulated in Table 4.9, along with the % of reduction in the peak absorbance A_{875}/A_{835}. Note that the % reduction in A_{875}/A_{835} given in Table 4.9 reflects only the relative amount of epoxide groups consumed during blending, but not the absolute quantity.

Table 4.9: FTIR peak absorbance A_{875}/A_{835} of ENR50/Alkyd blend series and % reduction in A_{875}/A_{835}

Blend	Blending time (t) /hr	A_{875}/A_{835}	% reduction in A_{875}/A_{835}[a]
ENR50/AlkydCO	0.08	6.70	0.53
	12	6.67	
ENR50/AlkydMA1	0.08	6.48	3.18
	12	6.27	
ENR50/AlkydMA2	0.08	6.59	5.11
	12	6.26	

[a] % reduction of $A_{875}/A_{835} = 100 \times [1-(A_{875}/A_{835})_{t=12}/(A_{875}/A_{835})_{t=0.08}]$

% reduction in A_{875}/A_{835} is the highest in ENR50/AlkydMA2 blend, presumably due to the higher amount of –COOH groups present in the system during blending. The trend in the % reduction of A_{875}/A_{835} is in line with the amount of –COOH groups present in the alkyd prior to blending. AlkydCO which has the least amount of –COOH groups among all the alkyds shows only marginal decrease in A_{875}/A_{835} when it was blended with ENR50. However, modification alkyd through incorporation of MA into AlkydCO chain has increased the reactivity of AlkydMA1 and AlkydMA2 towards ENR50 during blending. The results agree with the proposed reaction in Figure 4.18 where –COOH groups of alkyd are responsible for the reduction of epoxide groups in the blend through formation of ester linkages.

(b) Gel content

The extent of crosslink in the blends is reflected by the % of gel that is formed after soaking the blend in toluene for a period of 24 hours. Individually, all the alkyds and ENR50 are readily soluble in toluene, with the former recorded 100 % solubility while the latter shows 98 % solubility at ambient temperature. However, after ENR50 was blended with alkyds, it is able to resist total dissolution and considerable amount of gel which is insoluble in toluene was observed. This indicates that extensive network of crosslink was formed during blending of ENR50 and alkyd at ambient temperature. Figure 4.19 shows the change in gel content in the 3 series of ENR50/Alkyd blends as a function of blending time. Note that the initial % of gel (blending time= 0 minute) that is present in the 3 blend series corresponds to the gel content of ENR50 as alkyd is completely soluble in toluene.

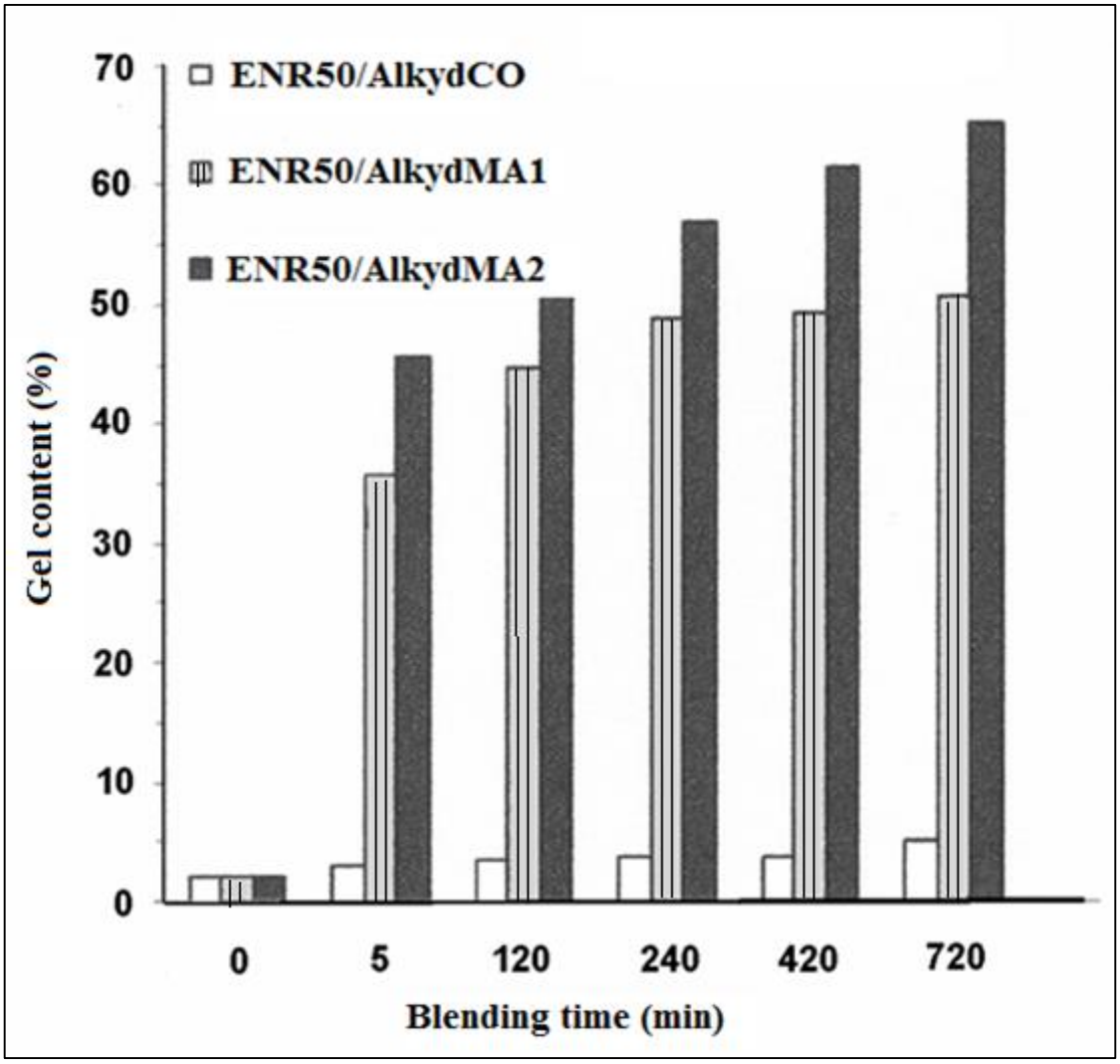

Figure 4.19: Variation of gel content with blending time in ENR50/AlkydCO, ENR50/AlkydMA1 and ENR50/AlkydMA2 blend series

Gel content of ENR50/AlkydCO blend series remain low, < 10 %, over different blending times owing to the low amount of –COOH groups in AlkydCO which could be insufficient to promote crosslinking in the blend. However, the gel content in the blend is still higher than the individual ENR50, presumably due to the grafting of AlkydCO on the rubber chain and polar interactions induced by the free –OH groups of AlkydCO with the epoxide groups of ENR50. Gel content of the blends agrees with the FTIR results where degree of crosslink in the blend is dependent on the amount of –COOH groups present in the alkyd. For example, within a short period of blending, 5 minutes,

the amount of gel in ENR50/AlkydMA1 blend has increased by 33 % while for ENR50/AlkydMA2 the amount of gel obtained is higher, 45 %.

(c) DSC analysis

DSC thermograms of ENR50/Alkyd mixture which have been blended for 5 minutes and 12 hours are shown in Figure 4.20. T_g of the blend was obtained from the midpoint of inflection in the curve and was tabulated in Table 4.10, along with T_g of ENR50 and alkyds. A single T_g was observed in each blend and this suggests the presence of a miscible amorphous phase, formed by the amorphous fraction of the semi-crystalline polymer (alkyd) and amorphous polymer (ENR50) (Prolongo et al., 2002). Melting transition from the crystalline fraction of alkyd however was unnoticeable in the thermograms, presumably most of the alkyd incorporated was consumed in the reaction with ENR and only negligible amount of free alkyd are left (if any).

Table 4.10: Glass transition temperature of ENR50, alkyds and ENR50/Alkyd blend series

Sample	Blending time /hr	T_g / °C
ENR50	-	-19.3
AlkydCO	-	-21.7
AlkydMA1	-	-21.5
AlkydMA2	-	-21.7
ENR50/AlkydCO	0.08	-20.6
	12	-20.6
ENR50/AlkydMA1	0.08	-20.0
	12	-18.7
ENR50/AlkydMA2	0.08	-19.8
	12	-17.8

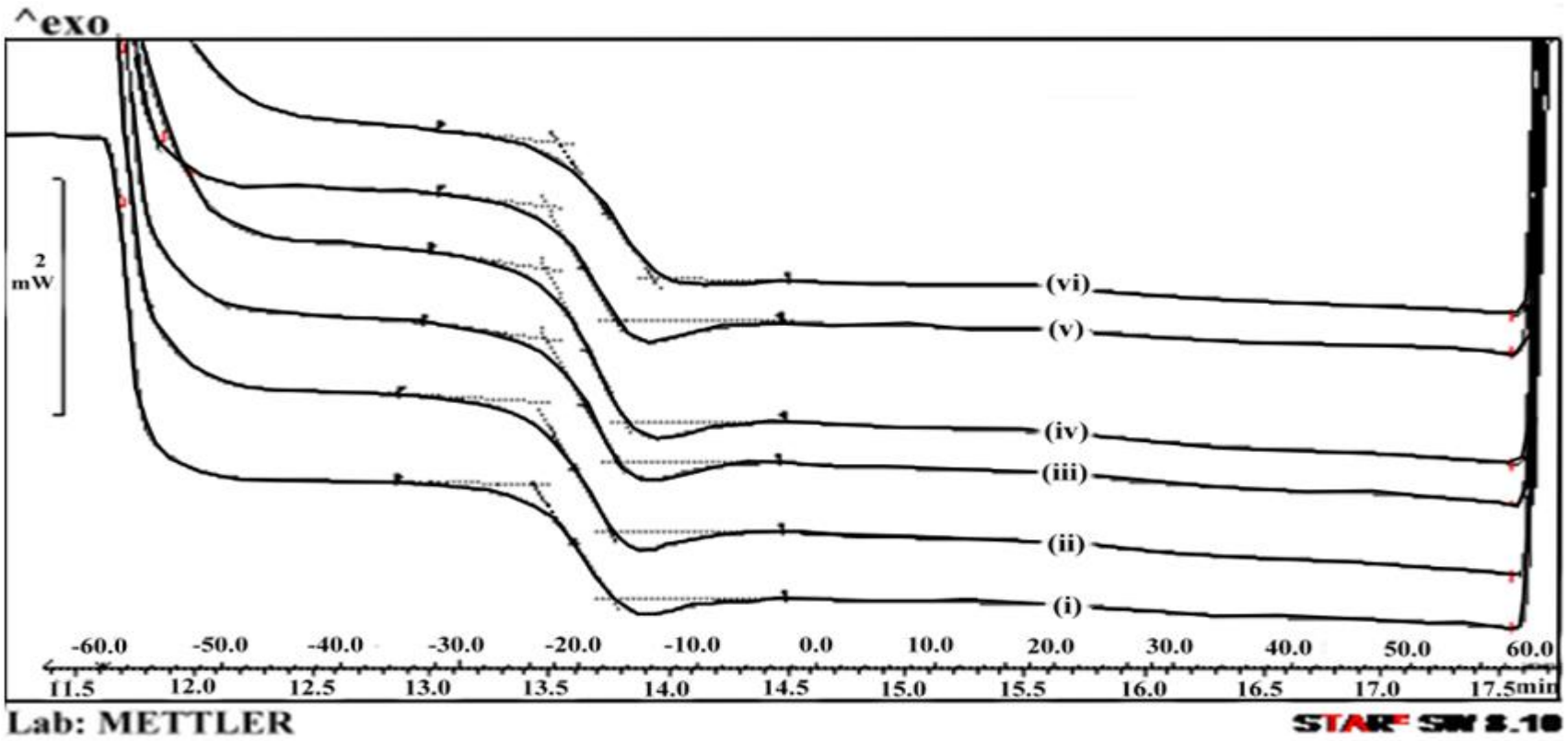

Figure 4.20: DSC thermograms of ENR50/Alkyd blend series: (i) ENR50/AlkydCO blend, blended for 5 minutes, (ii) ENR50/AlkydCO blend, blended for 12 hours, (iii) ENR50/AlkydMA1 blend, blended for 5 minutes, (iv) ENR50/AlkydMA1 blend, blended for 12 hours, (v) ENR50/AlkydMA2 blend, blended for 5 minutes, and (vi) ENR50/AlkydMA2 blend, blended for 12 hours

T_g of ENR50/AlkydCO blend series appear intermediate between those of the rubber and AlkydCO. This is not surprising as the blend comprised of 10 parts of alkyd per 100 parts of ENR50, and the T_g of the individual blend components are close to each other. However, this is not the case for ENR50/AlkydMA1 and ENR50/AlkydMA2 mixtures that have been blended for 12 hours as their T_g are higher than their pure components. The positive shift in T_g is due to reduced segmental mobility imposed by the increased interaction between the blend components. The MA-modified alkyds function as crosslinker in the system, linking the rubber chain together through formation of ester linkages with the epoxide groups. Besides, contribution from polar interactions between the functional groups in the blends is not ruled out. The –COOH groups in the alkyd could induce polar interactions with other -COOH groups (from pendant chains), -OH groups (from ring-opened products) or epoxide groups, resulting with increase in the T_g of the blends.

Note that the T_g shown in Table 4.10 are the T_g of the whole blend. It is not unusual to expect some unreacted components in the blends which could have caused the T_g of the blend to appear lower than actual. In order to confirm this, DSC measurement were carried out on ENR50/AlkydMA2 whole blend (blending time =7 hours) and the gel fraction of the same blend which has been soaked in toluene for 24 hours. T_g of ENR50/AlkydMA2 whole blend is observed at -18.9 °C. However, T_g recorded for the dried gel which has been soaked in toluene is higher, at -17.6 °C. The shift in T_g indicates that there is indeed presence of unreacted components in ENR50/AlkydMA2 whole blend. After immersion in toluene, some of the unreacted components were separated out from the blend as sol fraction, while the highly crosslinked structure in the blend appear as gel.

4.5.3 Analysis on sol portion of ENR50/AlkydMA2 blend

Sol fraction of ENR50/AlkydMA2 blend were analysed by FTIR and GPC in order to confirm the presence of unreacted components in the whole blends. Figure 4.21 shows the IR spectrum of the sol portion of ENR50/AlkydMA2 blend (blending time = 7 hours), which contains characteristic peaks of ENR50. This suggests that some of the unreacted rubber could have dissolved out into toluene during the immersion of the whole blend in the solvent. This is not unexpected as the blend was formulated with high ratio of epoxide groups (ENR50) to –COOH groups (AlkydMA2). Absorption bands representing the ester linkages in alkyd were observed at 1736 cm^{-1} (C=O stretching of ester group) and 1186 cm^{-1} (C-O stretching of ester group), indicating the presence of unreacted alkyd or low molecular weight ENR grafted with alkyd, that have dissolved to form the sol.

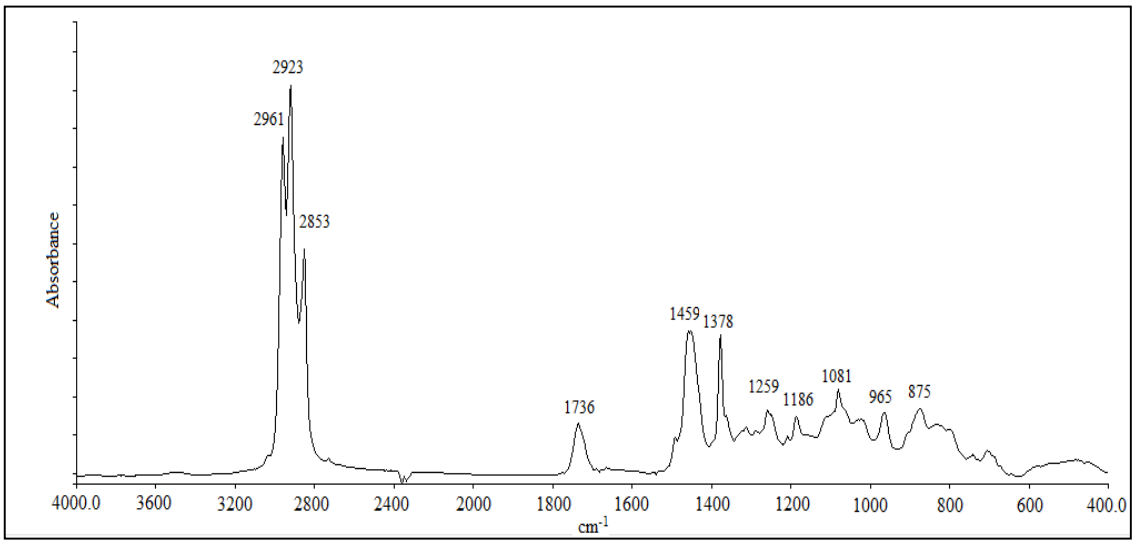

Figure 4.21: FTIR spectrum of sol portion of ENR50/AlkydMA2 blend (blending time = 7 hours)

Figure 4.22 shows the molecular weight distribution curves of dissolved ENR50, AlkydMA2, and the sol portion of ENR50/AlkydMA2 blend (blending time = 7 hours), along with their average molecular weights determined from GPC analysis. The individual blend components show a unimodal distribution of molecular weight with the dissolved ENR50 recorded a M_n of 112 753 g mol^{-1} and polydispersity of 3.4 while AlkydMA2 has a M_n of 1475 g mol^{-1} and a polydispersity of 1.4. On the other hands, the distribution curve of the sol portion of ENR50/AlkydMA2 blend is bimodal with a broad peak representing the higher molecular weight fraction and a narrow peak representing a lower molecular weight fraction. This is in agreement with the earlier discussion where the sol portion of the blend is made up of mixture of oligomers, in which the former could be contributed by the unreacted ENR50 or low molecular weight ENR50 grafted with alkyd, while the latter could be due to the unreacted alkyd present in the blend. Results from the FTIR and GPC analyses on the sol fractions agree that there are unreacted components present in the blend, and removal of those components has resulted with further increase in the T_g of the blend.

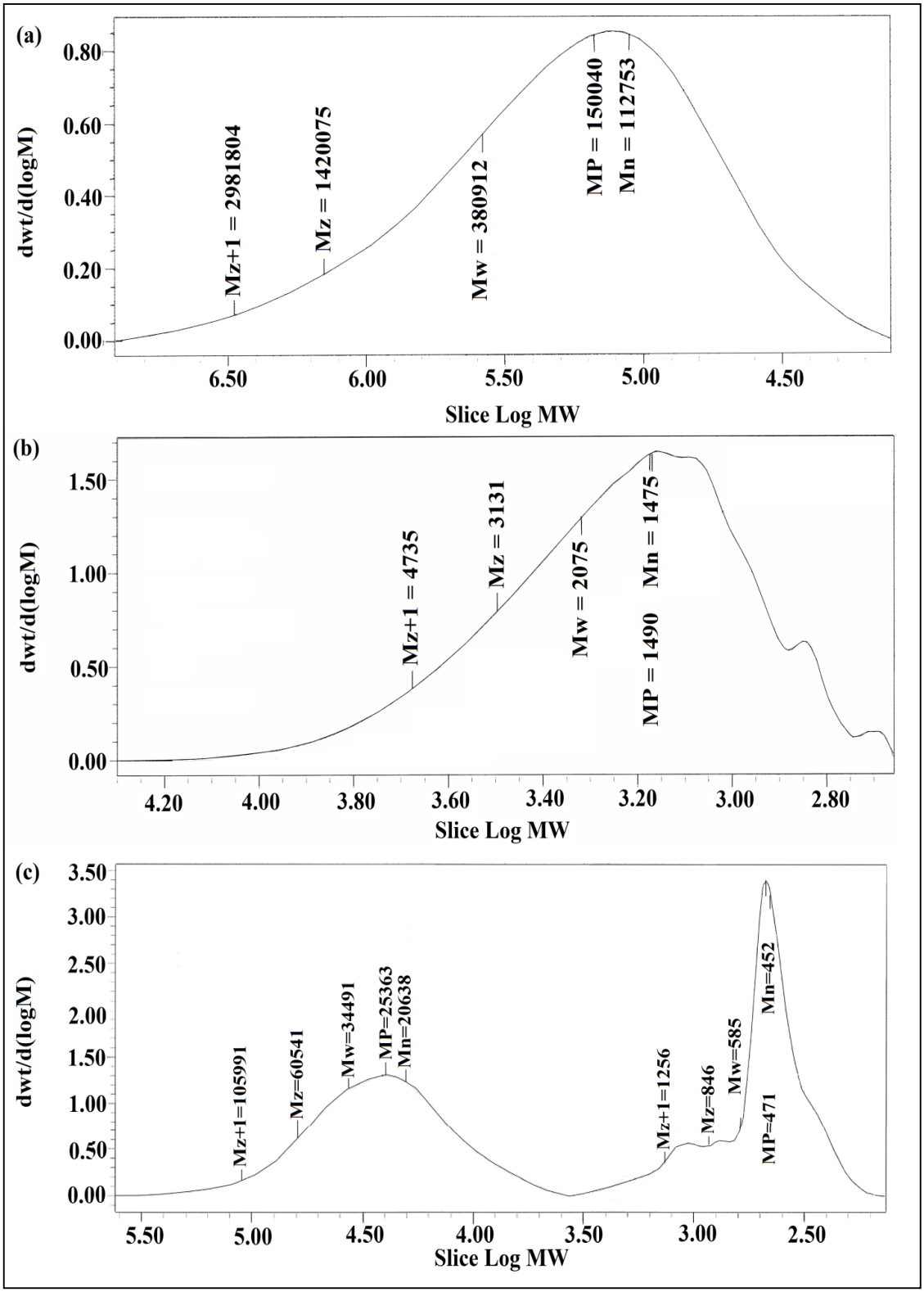

Figure 4.22: Molecular weight distribution curves of (a) Dissolved ENR50, (b) AlkydMA2, and (c) sol fraction of ENR50/AlkydMA2 blend (blending time= 7 hours)

4.6 Characterisation and properties of ENR50/Alkyd blends: Comparison of reaction between PA-modified alkyd and MA-modified alkyd with ENR50

4.6.1 FTIR analysis

Figure 4.23 shows the normalised FTIR spectra of ENR50/AlkydMA1 blend series and ENR50/AlkydPA1 blend series. The peaks in the spectra were normalised against the peak at 835 cm^{-1} for better comparison. Both the blend experienced reduction in the epoxide content when being blended from 5 minutes to 12 hours due to formation of crosslink between the epoxide group and the –COOH group in alkyd. Interestingly, the extent of ring opening of the epoxide group in ENR50/AlkydMA1 blend series are relatively higher as compared to ENR50/AlkydPA1 blend series. This is supported by the % reduction in A_{875}/A_{835} where ENR50/AlkydMA1 blend series show a reduction of 3.18 % when the blending time was prolonged from 5 minutes to 12 hours but ENR50/AlkydPA1 blend series reduced by 2.13 % only for the same period of blending.

Despite having similar amount of –COOH group in their chain, 8.0×10^{-4} mol g^{-1} alkyd, both AlkydMA1 and AlkydPA1 show different reactivity in the reaction with ENR50. In AlkydPA1, the -COOH incorporated into the alkyd is in the form of –OOC-Ph-COOH, where Ph = aromatic ring whereas the acid side chain in AlkydMA1 has the structure –OOC-CH=CH-COOH. Presence of the bulky aromatic ring could have contributed to steric hindrance in the reaction between the –COOH of AlkydPA1 and epoxy group of ENR50, thus effectively reduced the reactivity of the grafted –COOH.

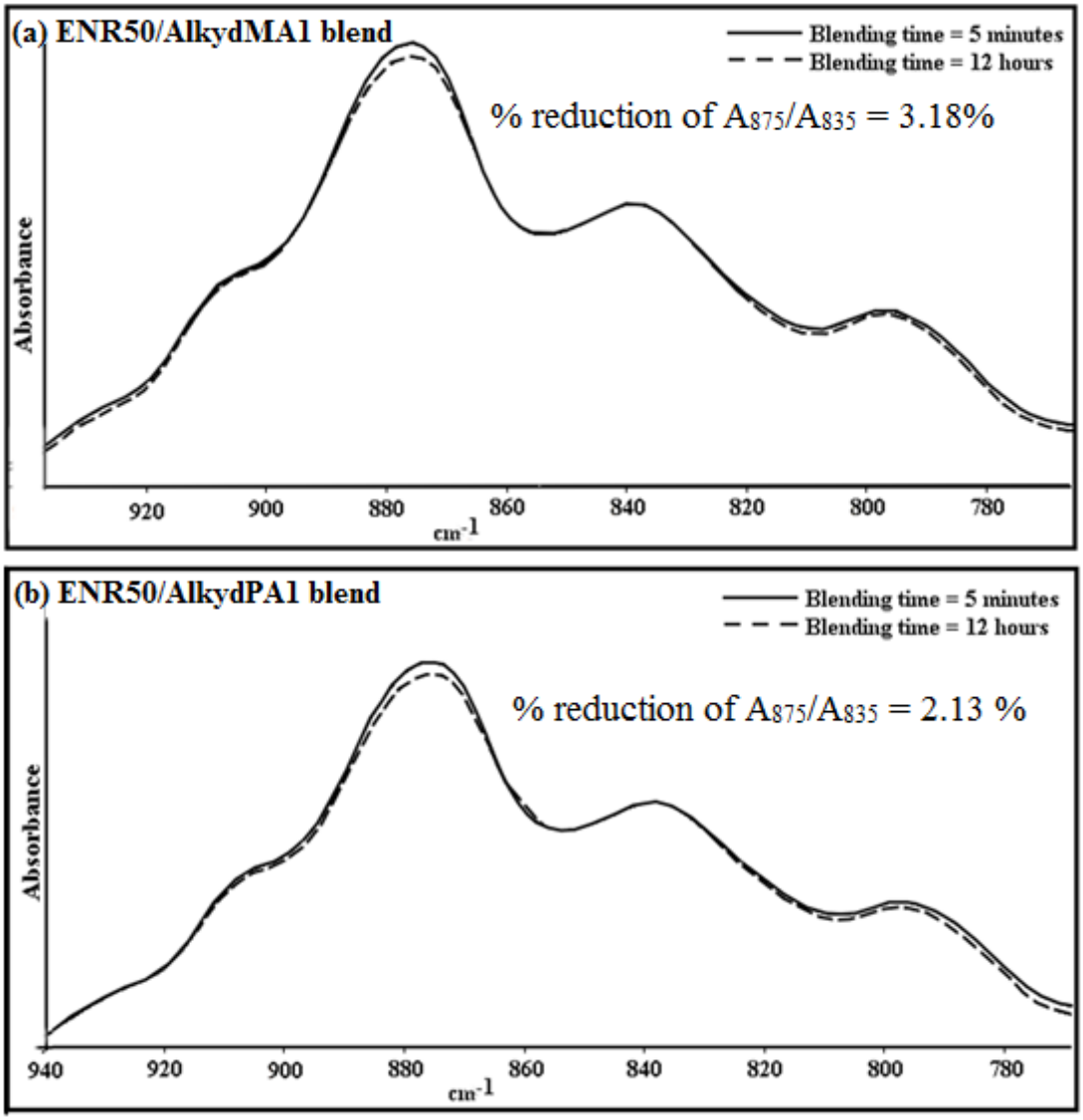

Figure 4.23: Normalised FTIR spectra of ENR50/AlkydMA1 and ENR50/AlkydPA1 blend series

4.6.2 Gel content

Figure 4.24 shows the variation of gel content in ENR50/AlkydMA1 and ENR50/AlkydPA1 blend series at different blending time. Note that the initial % of gel (blending time = 0 minute) that is present in the blend corresponds to the gel content of ENR50 as alkyd is completely soluble in toluene. Both the blend series show increasing trend in their gel content when the blending time was prolonged. This is related to the increase in the extent of crosslink in the blend leading to greater formation of gel which insoluble in toluene.

In the first 5 minutes of blending, rate of crosslinking in the blend was high leading to significant amount of gel formed in the blend. This is not totally unexpected as high amount of functional groups at the initial stage of blending increases the probability of ring-opening reaction of epoxide group by the –COOH groups from alkyd. The rate of crosslinking however started to slow down after 5 minutes of blending and became constant at the 7^{th} hour of blending. This may be due to the depletion of the available functional groups in the blends hence reduces the chances of crosslinking.

Over the different intervals of blending time, from 5 minutes to 12 hours, it can be observed that the gel content of ENR50/AlkydMA1 blend series are marginally higher compared to that of ENR50/AlkydPA1 blend series. For example, after blending for 4 hours, % of gel obtained from ENR50/AlkydMA1 blend is 48.9 % while ENR50/AlkydPA1 blend contains only 43.9 % of gel which insoluble in toluene. This agrees well with the FTIR results where alkyd with maleic acid side chain is slightly more reactive compared to those with phthalic acid side chain towards reaction with ENR50.

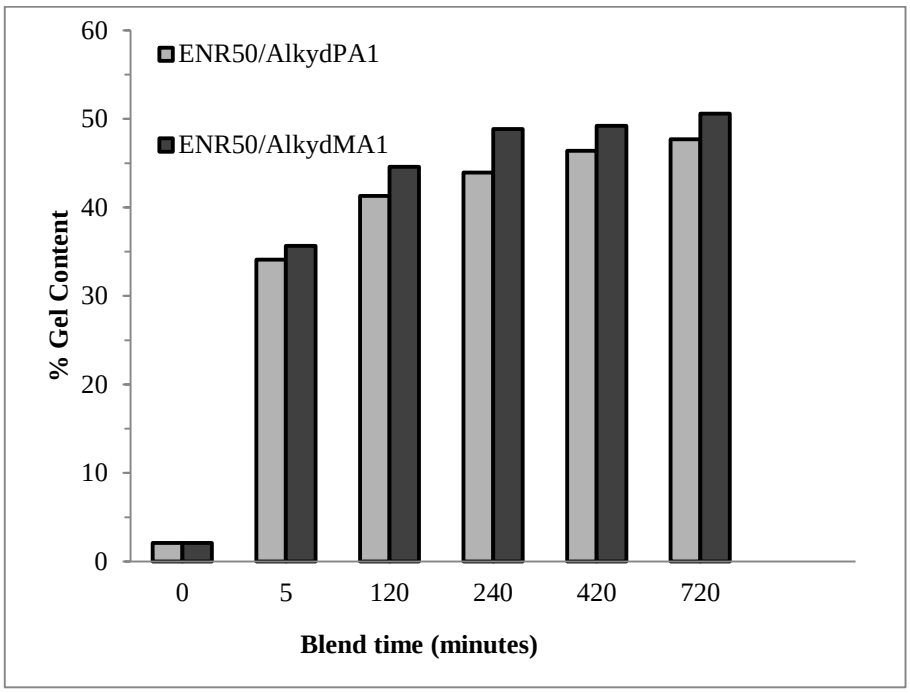

Figure 4.24: Variation of gel content in ENR50/AlkydMA1 and ENR50/AlkydPA1 blend series at different blending time

4.6.3 Thermal analysis

Thermal stability of polymer blend generally refers to the tolerance of the blend towards thermal decomposition, and it is frequently related to crosslink density and crosslinking structures in the compound. Various research papers have investigated the influence of degree of crossslinking in a polymer towards its thermal stability but with contradictory results. The correlation between crosslinking and thermal stability for methyl methacrylate cross-linked with various dimethacrylates and styrene crosslinked with divinylbenzene was studied by Wilkie and his research groups (1999). It was found that crosslinking degree did not always enhance the thermal stability of polymers. Highly crosslinked methyl methacrylate-dimethacrylate polymers did not show any improvement in their thermal stability whereas crosslinked polymers based on styrene-divinylbenzene show significant enhancement in thermal stability and increase in char formation relative to the increase in crosslink density. In an unrelated work, Wilkie and

his companion (2000), proposed that the type of crosslink is more important than the number of crosslinks in determining the thermal stability of crosslinked polymers. Different nature of crosslinks may have different degradation pathways, and therefore changes the onset temperatures of degradation.

Thermal degradation of ENR50/AlkydMA1 blend series and ENR50/AlkydPA1 blend series (blend composition = 10 parts of alkyd per 100 parts of ENR50) in this work were studied using TGA. The mass loss of the blends at specific heating rate under nitrogen atmosphere is shown in Figure 4.25. Initial decomposition temperature, T_i, which corresponds to temperature at 1 % decomposition, was empirically taken as an index to compare their thermal stability and the results are shown in Table 4.11. As seen from the T_i value in both the blend series, the onset temperature of degradation for the blends have significantly increased with the blending time. Mixture that have been blended for a longer time could form greater network of crosslinking. The results suggest that the formation of crosslinked structure in the blend has enhanced the thermal stability of the polymer as it reduces the molecular mobility, and increases the number of bonds that must be broken in order to observe mass loss.

T_i values of the blend series also reveals that ENR50/AlkydMA1 blend series have better tolerance towards thermal decomposition compared to ENR50/AlkydPA1 blend series. For example, ENR50/AlkydPA1 mixture after it was blended for 7 hours, started to show 1 % loss in its total weight at temperature 277.5 °C, whereas ENR50/AlkydMA1 blend which was prepared under the same condition and blending time recorded T_i value of 303.8 °C. The higher thermal stability in ENR50/AlkydMA1 blend series may be attributed to the higher fraction of crosslinking regions in the polymers presumably due to the higher reactivity of alkyd with maleic acid side chain to react with the epoxy group in ENR50 as compared to the alkyd with phthalic acid side chain.

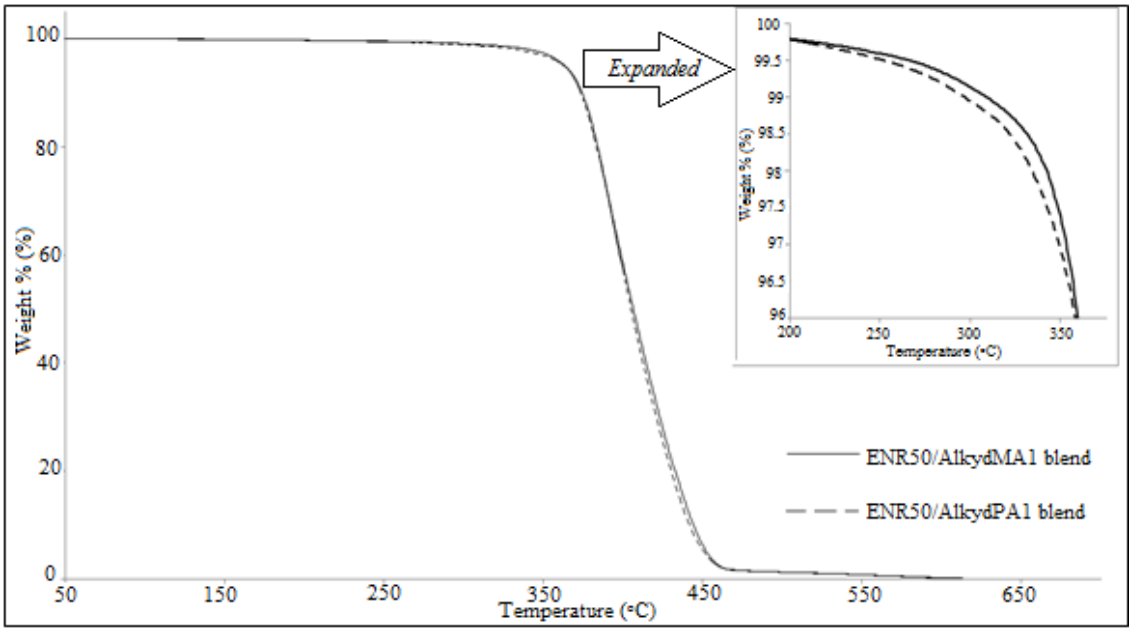

Figure 4.25: Overlay TG curve of ENR50/AlkydMA1 and ENR50/AlkydPA1 blends, blended for 12 hours at heating rate of 30 °C/min

Table 4.11: T_i of ENR50/AlkydMA1 and ENR50/AlkydPA1 blend series at different blending times

Blending time/ minutes	Temperature at 1 % decomposition, T_i / °C	
	ENR50/AlkydMA1 blend	ENR50/AlkydPA1 blend
5	285.9	273.1
120	294.7	275.9
240	302.7	276.5
420	303.8	277.5
720	330.6	305.7

a) Activation energy of degradation (E_d) using Kissinger equation

Kissinger's method of calculating E_d of thermal degradation processes is based upon a series of experiments in which small milligrams quantities of samples are subjected to multiple heating rates and the peak temperature, T_m where the rate of degradation is at maximum, is measured at each heating rate (Kissinger, 1957; Blaine & Kissinger, 2012). The equation is derived from a common fundamental kinetic equation where for a heterogeneous system under non-isothermal conditions, it is assumed that the rate of decomposition (dα/dt) is proportional to a function of the degree of conversion (f(α)) and temperature (T), and these two variables are independent ones (Sestak, 1984).

$$\frac{d\alpha}{dt} = kf(\alpha) \qquad (Eqn.\ 4.1)$$

The proportionality constant (k) is the decomposition rate constant, which can be expressed by the Arhenius equation, where R is the gas constant, A is the pre-exponential factor and E_d is the activation energy. The reaction rate equation (Eqn 4.1) and Arhenius equation are commonly combined into general rate equation:

$$\frac{d\alpha}{dt} = A\exp(\frac{-E_d}{RT})f(\alpha) \qquad (Eqn.\ 4.2)$$

If Eqn. 4.2 is differentiated by parts, we obtained:

$$\frac{d[d\alpha/dt]}{dt} = A\exp\left(\frac{-E_d}{RT}\right)\frac{d[f(\alpha)]}{dt} + A\,f(\alpha)\frac{d[\exp(-E_d/RT)]}{dt} \qquad (Eqn.\ 4.3)$$

By the usual change of the variable time into temperature $(\beta = dT/dt)$, d[exp (-E_d/RT)/dt = $E_d\beta/RT^2$ exp (-E_d/RT). At maximum rate of degradation, T = T_m, d[dα/dt]/ dt =0 and Eqn. 4.3 becomes

$$0 = \frac{d[f(\alpha)]}{dt} + f(\alpha)\frac{E_d \beta}{RT_m^2} \qquad (Eqn.\ 4.4)$$

Given the identity f'(α)= d[f(α)]/d(α) and d[f(α)]/dt = f'd(a)/dt. Substituting this into Eqn. 4.4, it can be obtained:

$$0 = A \exp\left(\frac{-E_d}{RT_m}\right) f'(\alpha) + \frac{E_d \beta}{RT_m{}^2} \qquad (Eqn.\ 4.5)$$

Solving for β/T_m^2 and taking the natural logarithm, Eqn. 4.5 can be expressed as

$$\ln\left[\frac{\beta}{T_m{}^2}\right] = \ln\left[\frac{ZR}{E_d}\right] + \ln[-f'(\alpha)] - \frac{E_d}{RT_m} \qquad (Eqn.\ 4.6)$$

If the reaction is assumed to be first order (n=1), then f'(α)= 1-α, and ln [-f'(α)]=0, and this gives the Kissinger equation:

$$ln\frac{\beta}{T_m{}^2} = ln\frac{AR}{E_d} - \frac{E_d}{RT_m} \qquad (Eqn.\ 4.7)$$

The apparent activation energy, E_d and pre-exponential factor, A can be calculated from the slope and intercept of the straight line generated from the plot of ln (β/ T_m^2) against $1/ T_m$ (Lee et al., 2001; Sivalingham et al., 2004).

DTG curves of ENR50/AlkydMA1 blend and ENR50/AlkydPA1 blend are shown in Figure 4.26. The blends used are those that have been blended for 7 hours. It can be observed that the peak temperature, T_m which is the temperature at maximum degradation rate in the DTG curves shifts to higher values with increasing heating rate. Similar results are observed for both the blend series of different blending times. The plots of ln (β/ T_m^2) against 1/ T_m for the two series of blends are shown in Figure 4.27. The apparent activation energy of degradation, E_d and pre-exponential factor, A were calculated from the slopes and intercepts of the straight lines generated from the plots and the results are summarised in Table 4.12 and Table 4.13.

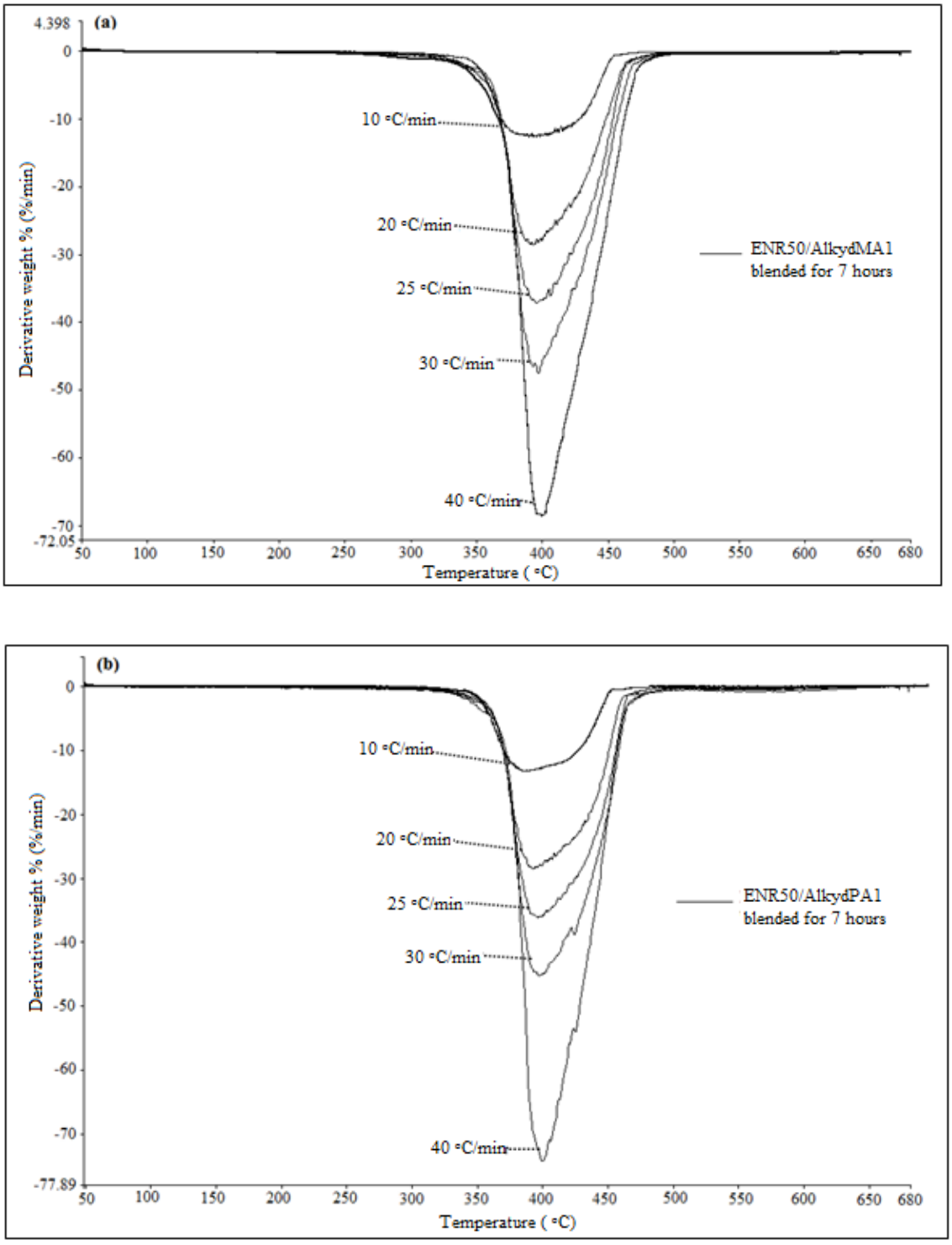

Figure 4.26: DTG curves of (a) ENR50/AlkydMA1 and, (b) ENR50/AlkydPA1 blends, blended for 7 hours

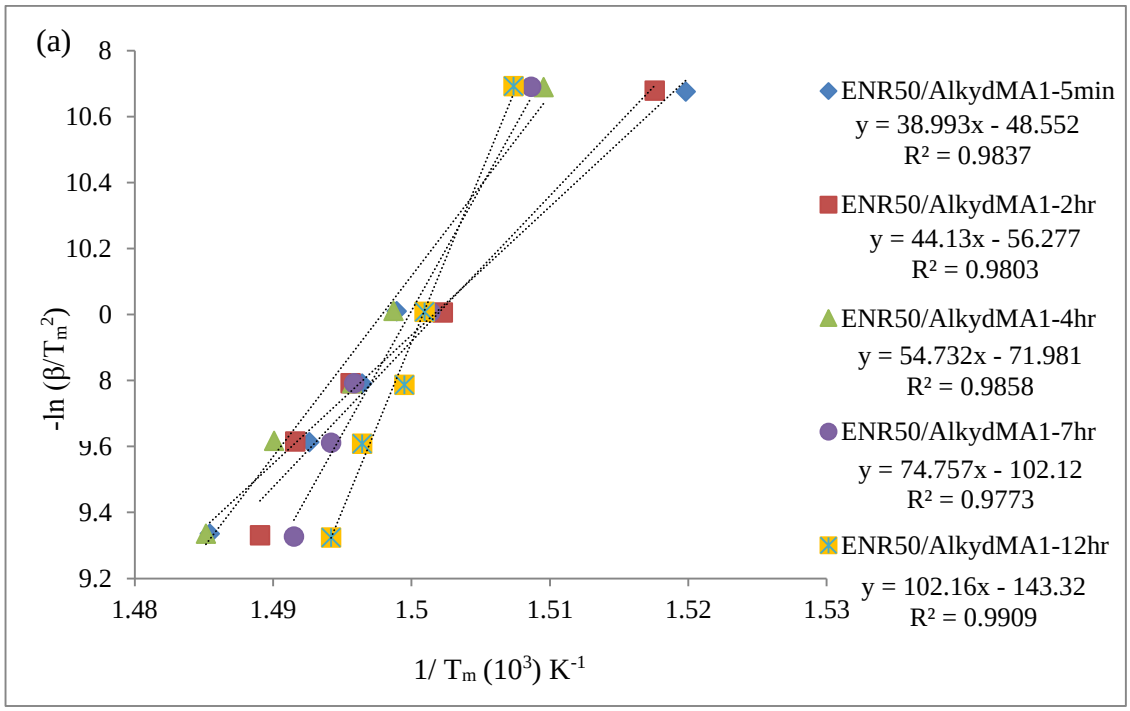

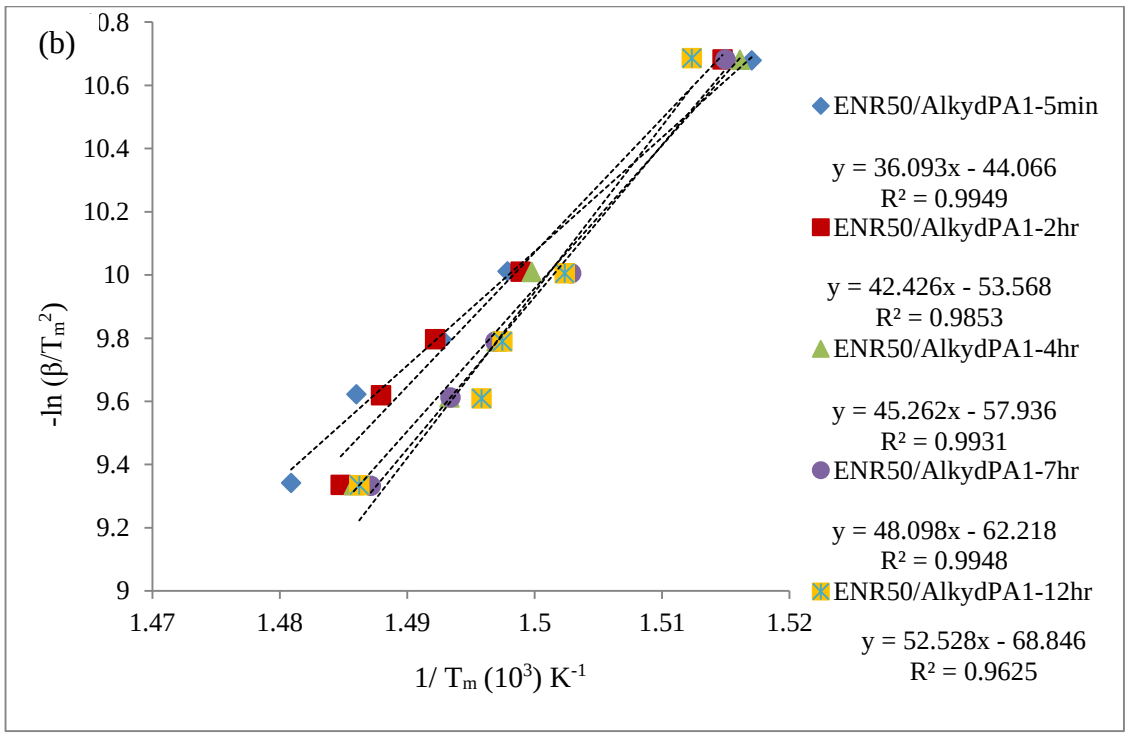

Figure 4.27: Dependence of –ln (β/T_m^2) on 1/ T_m for non-isothermal degradation of (a) ENR50/AlkydMA1 blend series and (b) ENR50/AlkydPA1 blend series (Kissinger equation)

Table 4.12: Values of kinetic parameters for non-isothermal degradation of ENR50/AlkydMA1 blends (composition: 10 parts of AlkydMA1 per 100 parts of ENR50) determined by Kissinger method

Blend	Blending time (hours)	Heating rate, β ($K\ min^{-1}$)	T_m (K)	E_d ($kJ\ mol^{-1}$)	A (s^{-1})
ENR50/AlkydMA1	0.08	10	657.98	324.2	4.72×10^{22}
		20	667.14		
		25	668.26		
		30	669.96		
		40	673.21		
ENR50/AlkydMA1	2	10	658.95	366.9	1.20×10^{26}
		20	665.66		
		25	668.63		
		30	670.42		
		40	671.57		
ENR50/AlkydMA1	4	10	662.45	455.0	9.90×10^{32}
		20	667.25		
		25	668.58		
		30	671.11		
		40	673.34		
ENR50/AlkydMA1	7	10	662.85	621.5	1.08×10^{50}
		20	666.06		
		25	668.51		
		30	669.26		
		40	670.46		
ENR50/AlkydMA1	12	10	663.41	848.8	1.73×10^{64}
		20	666.25		
		25	666.90		
		30	668.26		
		40	669.26		

Table 4.13: Values of kinetic parameters for non-isothermal degradation of ENR50/AlkydPA1 blends (composition: 10 parts of AlkydPA1 per 100 parts of ENR50) determined by Kissinger method

Blend	Blending time (hours)	Heating rate, β ($K\ min^{-1}$)	T_m (K)	E_d ($kJ\ mol^{-1}$)	A (s^{-1})
ENR50/AlkydPA1	0.08	10	659.18	300.0	4.90×10^{20}
		20	667.62		
		25	669.92		
		30	672.94		
		40	675.27		
ENR50/AlkydPA1	2	10	660.18	352.7	7.69×10^{24}
		20	667.16		
		25	670.16		
		30	672.07		
		40	673.50		
ENR50/AlkydPA1	4	10	659.59	376.3	6.48×10^{26}
		20	666.77		
		25	668.00		
		30	669.65		
		40	673.04		
ENR50/AlkydPA1	7	10	660.08	399.8	4.97×10^{28}
		20	665.40		
		25	668.04		
		30	669.61		
		40	672.43		
ENR50/AlkydPA1	12	10	661.23	436.7	4.11×10^{31}
		20	665.62		
		25	667.80		
		30	668.53		
		40	672.84		

Based on the calculated activation energies of degradation, E_d, there is improvement in thermal stability of the blends with increasing blending time. The trend in thermal stability may be due to the increase in crosslink density present in the blend which results in higher energy required for degradation. Besides, results from the kinetic parameters of the blends also show that ENR50/AlkydMA1 blend series (Table 4.12) have relatively higher thermal stability compared to ENR50/AlkydPA1 blend series (Table 4.13). At same blending time, E_d values of ENR50/AlkydMA1 blend series are higher compared to those of ENR50/AlkydPA1 blend series. It indirectly reflects the superiority of AlkydMA1 over AlkydPA1 as crosslinker in ENR50.

b) Activation energy of degradation (E_d) using Flynn-Wall-Ozawa method

Although Kissinger method is widely used in determining the kinetic parameters of degradation processes, there are however some limitations. One of the limitations of this method is the assumption of the same mechanism, and thus kinetic parameters, hold throughout the reaction. E_d determined at single point T_m may not be the same as the one observed earlier or later during the reaction. Hence, E_d calculated using Kissinger method gives the values of the overall E_d in the decomposition processes, which may constitute several mechanisms with different E_d (Sin et al., 2012).

Alternative kinetic methods, i.e. Flynn-Wall-Ozawa (FWO) methods which relates the E_d at any degree of conversion, α may be useful to probe the complexity of a decomposition mechanism (Popescu, 1996; Dowdy, 1987). This method is a relatively simple method which involves measuring the temperatures at fixed values of α, from experiment at different heating rates, β. The equation involved in FWO methods (Erceg et al., 2005) is shown in Eqn.4.8:

$$\log \beta = \log \frac{AE_d}{g(\alpha)R} - 2.315 - \frac{0.4567E_d}{RT} \qquad (Eqn.\ 4.8)$$

where:

g(α)= function of conversion

E_d= apparent activation energy of degradation (kJ mol^{-1})

A= pre-exponential factor

β= heating rate (°C min^{-1})

R= general gas constant (J $mol^{-1}K^{-1}$)

T= absolute temperature (K)

The plot of log β versus the reciprocal of absolute temperature, T at a given value of degree of decomposition will give a straight line. Apparent activation energy of degradation, E_d is calculated from the slopes of these lines for every degree of conversion.

FWO plots of ENR50, ENR50/AlkydMA1 blend and ENR50/AlkydPA1 blend (blend composition: 10 parts of alkyd per 100 parts of ENR50) which have been blended for 7 hours at various degree of conversion, α are displayed in Figure 4.28 (a)-(c) respectively. The E_d values for the decomposition of ENR50 and ENR50/Alkyd blends were determined in the conversion range of $0.1 \leq \alpha \leq 0.9$ which corresponds to temperature range of decomposition studied i.e. from 300 to 500 °C.

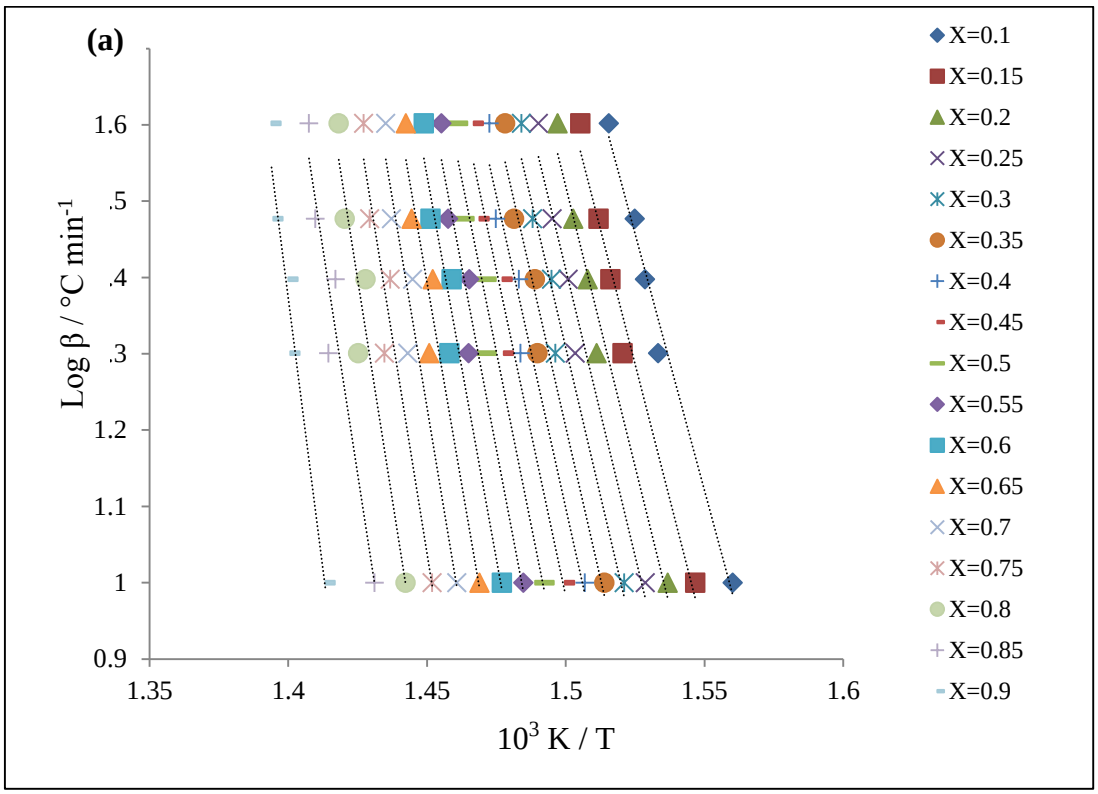
(a)
Log β / °C min-1
1.6
.5
.4
.3
1.2
1.1
1
0.9
1.35
1.4
1.45
1.5
1.55
1.6
10^3 K / T
X=0.1
X=0.15
X=0.2
X=0.25
X=0.3
X=0.35
X=0.4
X=0.45
X=0.5
X=0.55
X=0.6
X=0.65
X=0.7
X=0.75
X=0.8
X=0.85
X=0.9

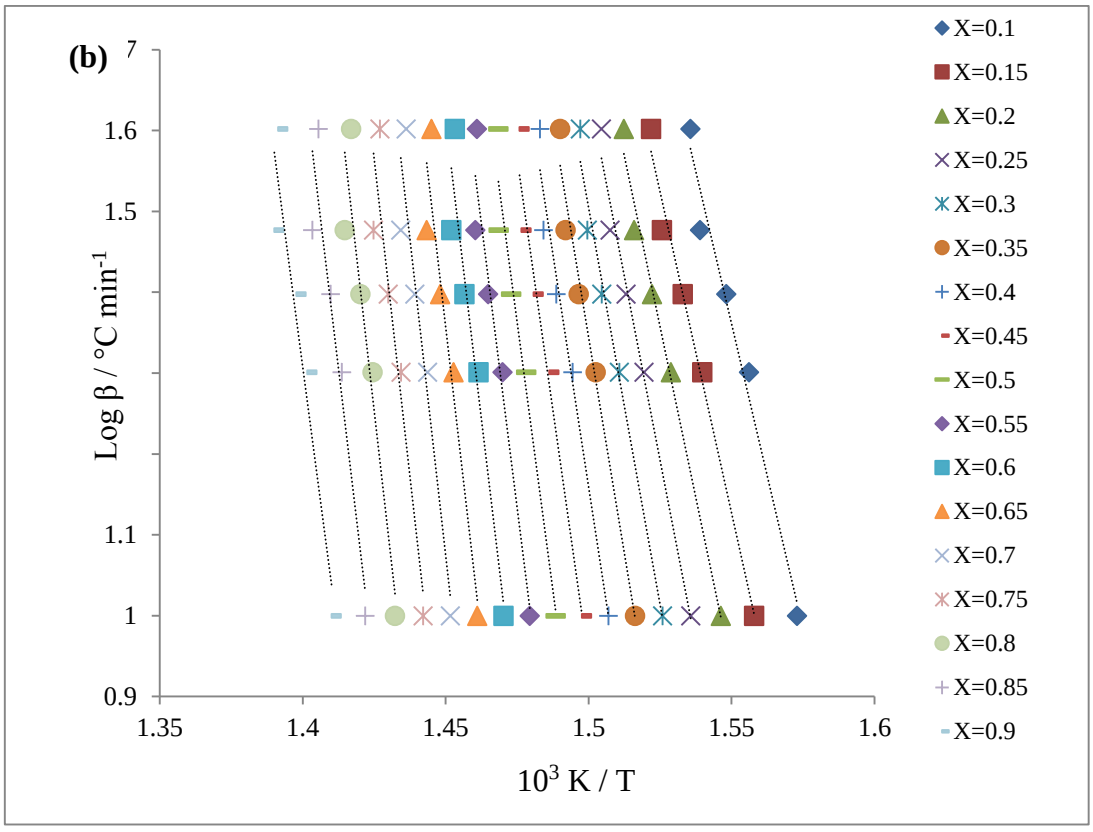
(b)
Log β / °C min-1
1.6
1.5
1.1
1
0.9
1.35
1.4
1.45
1.5
1.55
1.6
10^3 K / T
X=0.1
X=0.15
X=0.2
X=0.25
X=0.3
X=0.35
X=0.4
X=0.45
X=0.5
X=0.55
X=0.6
X=0.65
X=0.7
X=0.75
X=0.8
X=0.85
X=0.9

‘Figure 4.28, continued’

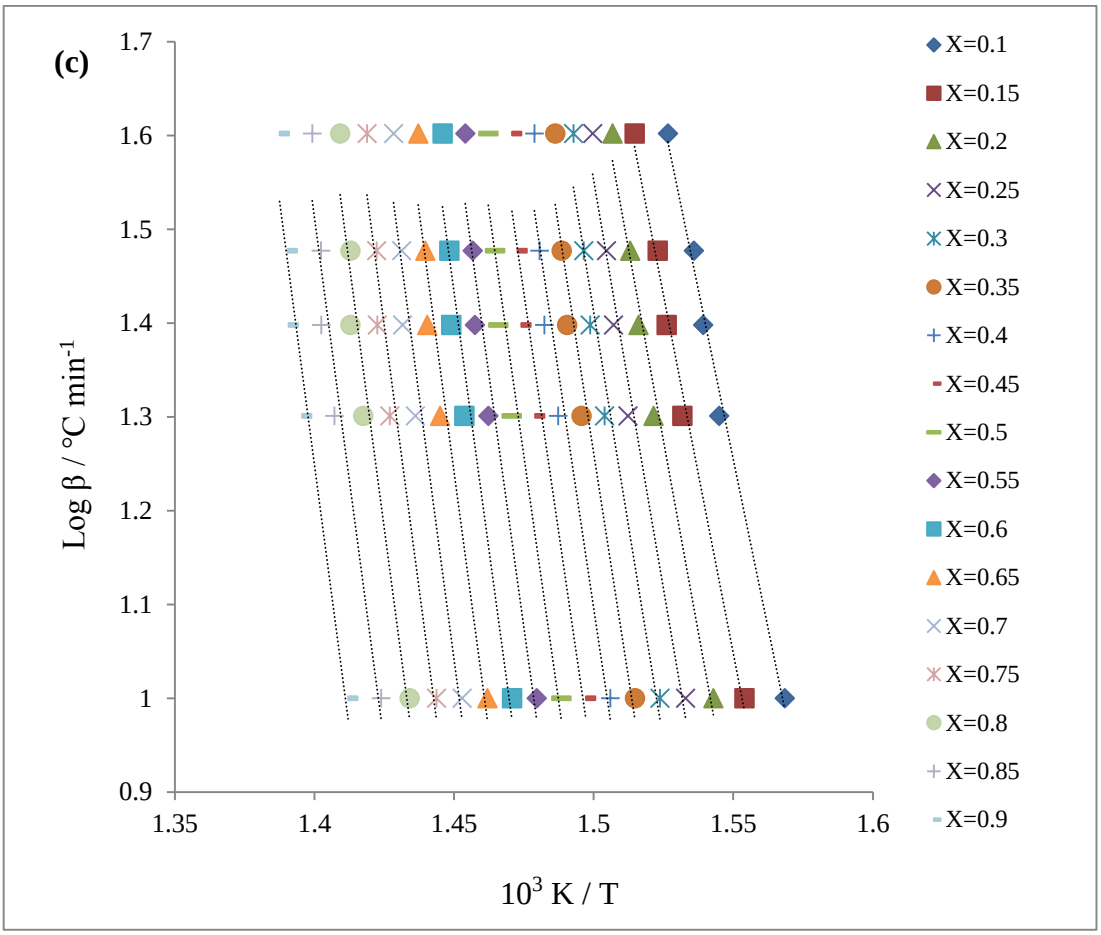

Figure 4.28: Flynn-Wall-Ozawa plots of (a) ENR50, (b) ENR50/AlkydMA1 blends, blended for 7 hours and (c) ENR50/AlkydPA1 blend, blended for 7 hours at varying degree of conversion, α.

Figure 4.29 shows the activation energies of degradation, E_d of the blends and ENR50 at various degree of conversions. Analysis on the results show that E_d of ENR50 is much lower compared to those of ENR50/AlkydMA1 and ENR50/AlkydPA1 blends. This implies the higher stability of the blends as a result of formation of crosslink between the epoxide groups of ENR50 and –COOH groups of alkyd. Also, ENR50/AlkydMA1 blend shows higher activation energy of decomposition as compared to that of ENR50/AlkydPA1 blend for all degree of conversion. The result agrees well with the E_d calculated from Kissinger method where greater extent of crosslink is formed in the former. As indicated in the previous discussion, the structure of acid side chains present in AlkydMA1 is in the form of –OOC-CH=CH-COOH, which is expected to experience less steric hindrance, thus easier for the -COOH to undergo reaction with the epoxide of ENR50.

For the thermal decomposition of ENR50, values of E_d are almost constant in the conversion range α= 0.10-0.90 and has no dependence on α. It can be concluded that the thermal degradation of ENR50 follows a simple reaction mechanism, where single stage thermal degradation took place. On the other hand, E_d values of ENR50/AlkydMA1 blend are in an increasing function of α in the conversion range of 0.10-0.75 where E_d increased from 274 to 574 kJ mol^{-1}. Beyond α= 0.75, E_d values started to drop and E_d= 485 kJ mol^{-1} at α= 0.90. Similar trend in E_d values ($0.10 \leq \alpha \leq 0.75$) were observed for thermal degradation of ENR50/AlkydPA1 blend where E_d increased from 262 to 409 kJ mol^{-1}. However, E_d remain constant at 409 kJ mol^{-1} with the subsequent degree of conversion. The dependence of E_d on α indicates that thermal degradation of the blends follow complex reaction mechanisms, which could involve several reaction mechanisms (Ataei et al., 2012).

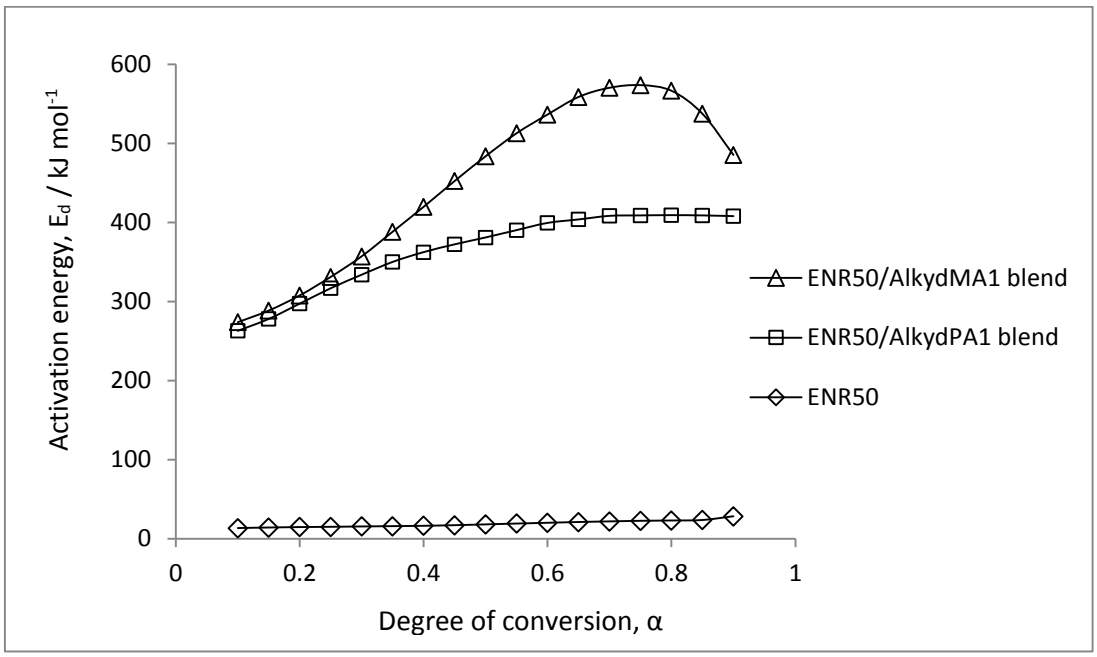

Figure 4.29: Plots of activation energy at various degree of conversion for ENR50, ENR50/AlkydMA1 and ENR50/AlkydPA1 blends

4.7 Development of UV-induced crosslinking in ENR50/AlkydMA1 blend

4.7.1 Reactions during UV irradiation

The principle method involved in the preparation of UV-curable elastomer is to introduce a photoinitiator that forms reactive species when irradiated, thus initiating chemical crosslinking via polymerisation of the monomers and oligomers in cationically or radically curable system. Benzophenone was chosen as the UV photoinitiator in this work owing to its low price and expected longer shelf-life of the end-product as compared to those formulated with highly reactive photoinitiators.

Figure 4.30 shows the IR spectra of EA-B0T0 and EA-B5T0 blends before irradiated with UV light. The spectra are quite similar to each other with peaks at 875 and 835 cm^{-1} representing the epoxide and C=C groups of the ENR50 unit, respectively, while others peaks at 3409, 1735, 1282 and 1060 cm^{-1} correspond to the characteristic peaks of AlkydMA1. Presence of benzophenone in EA-B5T0 blend is also shown in the spectra; appearance of strong peaks at 704 cm^{-1} (aromatic =C-H bending) and 1661 cm^{-1} (aromatic C=C stretching). Normalised FTIR spectra of the blends before (0 s), and after (240 s) UV irradiation are shown in Figure 4.31 and 4.32. Note that the peaks in the spectra were normalised against the peaks at 1456 cm^{-1} to overcome the effect of different film thickness during IR scan.

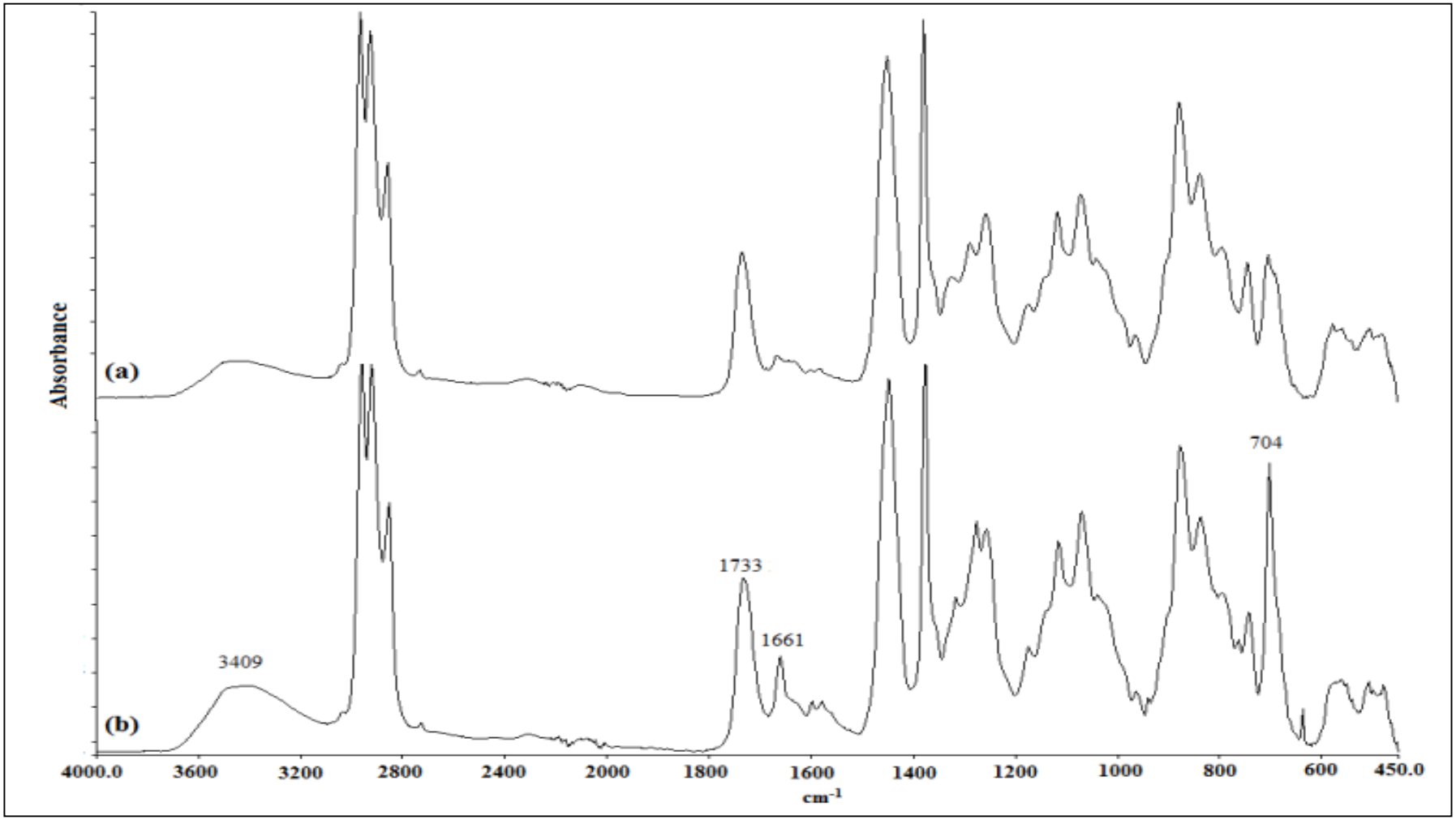

Figure 4.30: FTIR spectra of (a) EA-B0T0 blend and, (b) EA-B5T0 blend, before irradiated with UV light

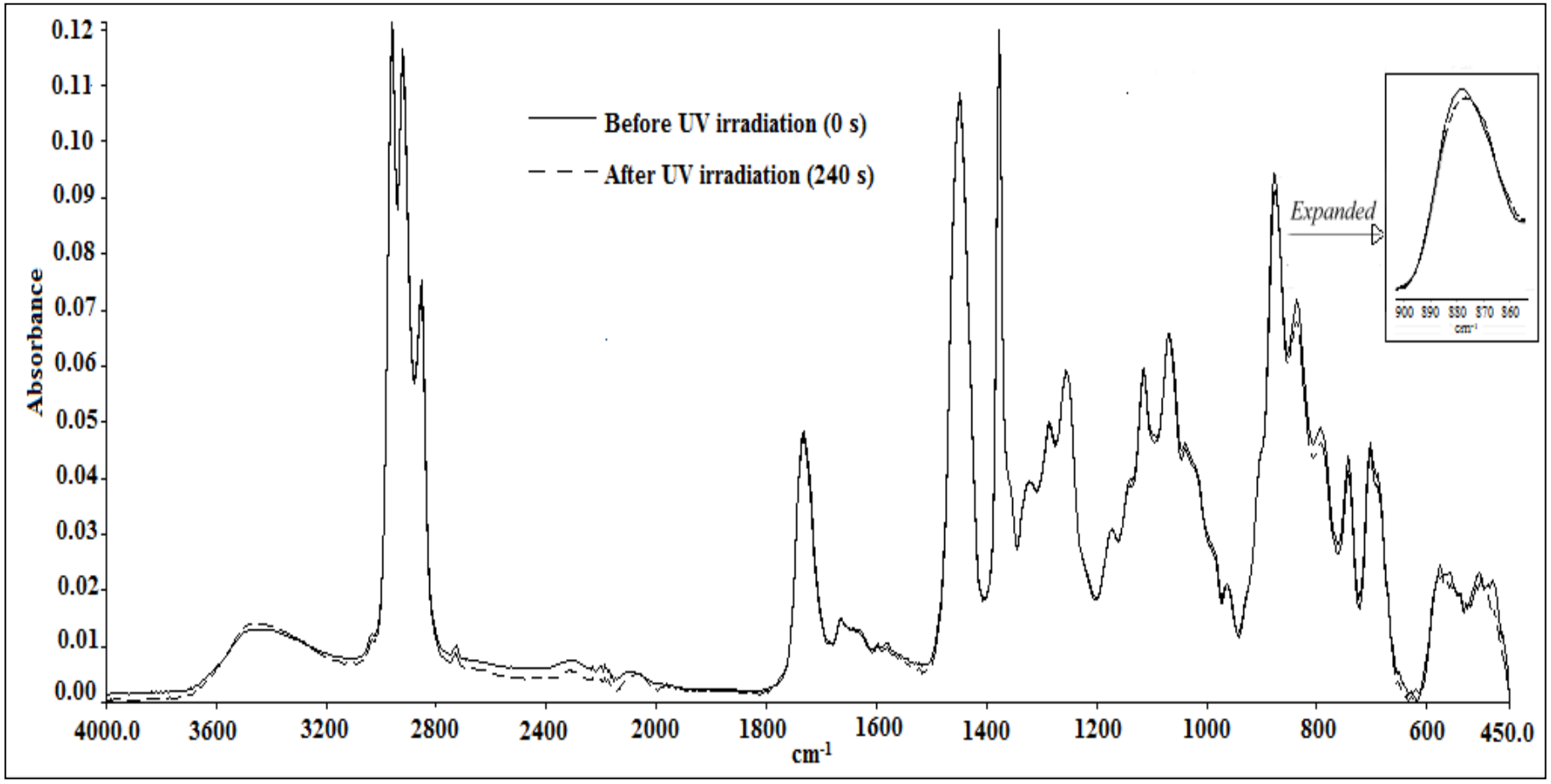

Figure 4.31: Normalised FTIR spectra of EA-B0T0 blend, before (0 s) and after (240 s) UV irradiation

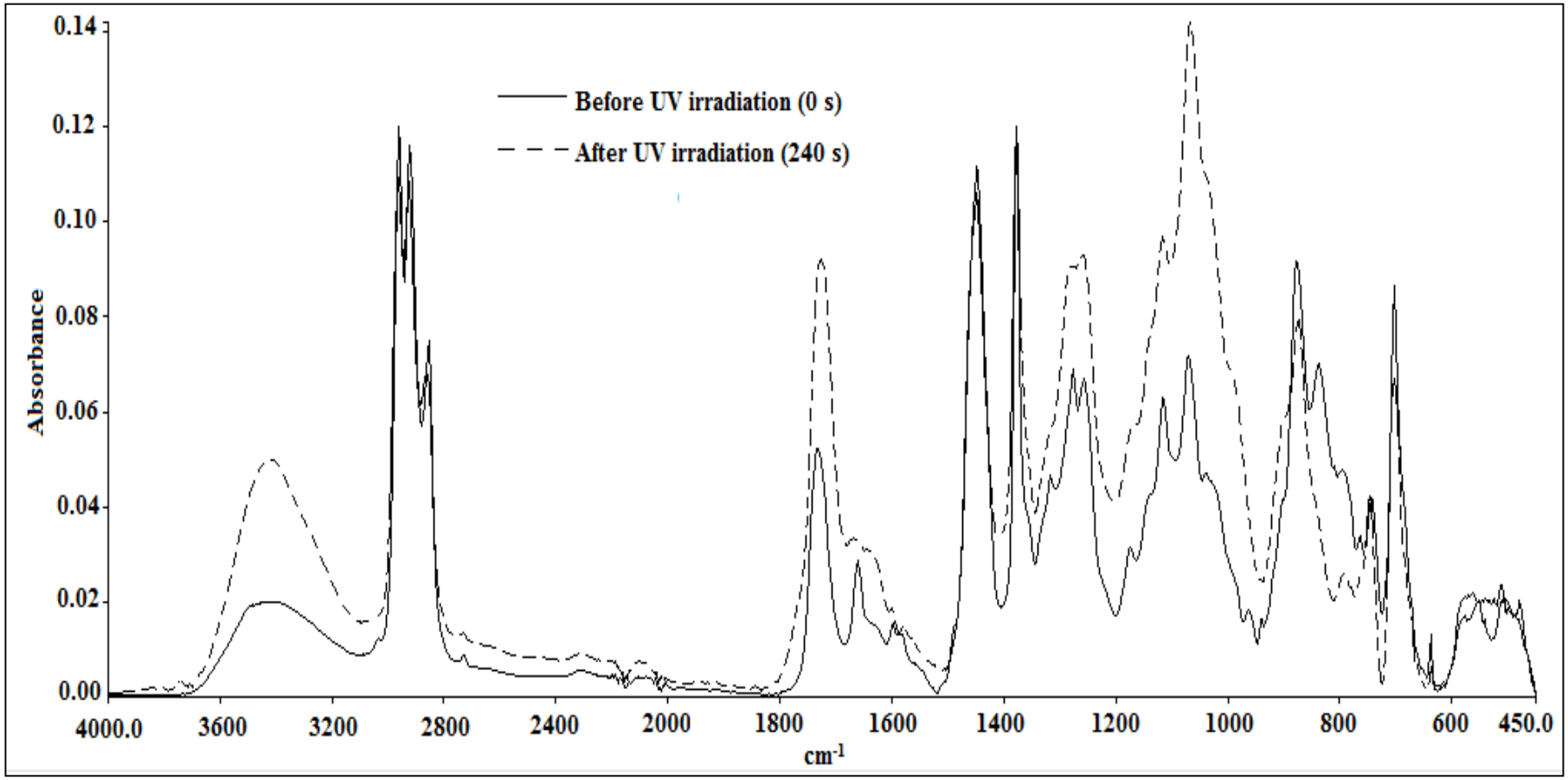

Figure 4.32: Normalised FTIR spectra of EA-B5T0 blend, before (0 s) and after (240 s) UV irradiation

Overall, no significance difference was observed in the IR spectra of EA-B0T0 blend, before and after UV irradiation, except for the peak at 875 cm^{-1} which has shown notable reduction after the blend was irradiated with UV light for 240 s. It is noteworthy that all the blends were dried to thin films prior to UV irradiation. The decrease in epoxide ring absorbance (875 cm^{-1}) is presumably due to the ring opening reaction of epoxide group by the –COOH group of alkyd at solid state, facilitated by the increase in temperature during exposure to UV light.

On the other hand, obvious changes were observed in the IR spectra of EA-B5T0 blend, before and after UV irradiation. Peaks at 835 cm^{-1} (C=C stretching of cis-1,4-polyisoprene unit in ENR50) and 1661 cm^{-1} (aromatic C=C stretching and C=C stretching of grafted MA in AlkydMA1) are no longer apparent after the blend was irradiated with UV light. The disappearance of these peaks indicates significant crosslink reaction involving the C=C group has taken place during UV irradiation. In addition, absorption bands which correspond to the O-H stretching and C-O stretching of the hydroxyl group at 3409 cm^{-1} and 1060 cm^{-1} respectively, experienced remarkable increase in their absorbance after UV irradiation. This was not unexpected as the incorporated benzophenone abstracts a hydrogen atom when irradiated with UV light to initiate the free radical reaction in the system. In the initiation stage, -C=O in benzophenone is converted to -C-OH.

The reaction that took place during UV irradiation is proposed in Figure 4.33. Benzophenone in EA-B5T0 blend is responsible to generate radicals to propagate crosslinking in the blend. When the photoinitiator absorbs a UV photon, it is excited to a short-lived singlet state and then relaxes to a more stable triplet state. Subsequently, it abstracts a hydrogen atom from the polymer backbone to generate a pair of radicals. The initiating free radical then attacks the ethylenic unsaturation of the oligomers in the system to form the initiated species. These initiated species then react with more

unsaturated site in the chain propagation step. Finally, the molecular chain is terminated by free radical recombination either through combination of non-initiating free radical species, or combination with initiated free radical species, or combination with another propagating molecule. Note that the ketyl radical generated during initiation does not participate in the chain propagating step. It decays into an inert species that does not enter into the polymerisation reaction, or acts as chain terminator. This is due to its limited capability of initiating or propagating polymerisation at the rapid rate required for radiation curing (Koleske, 2002).

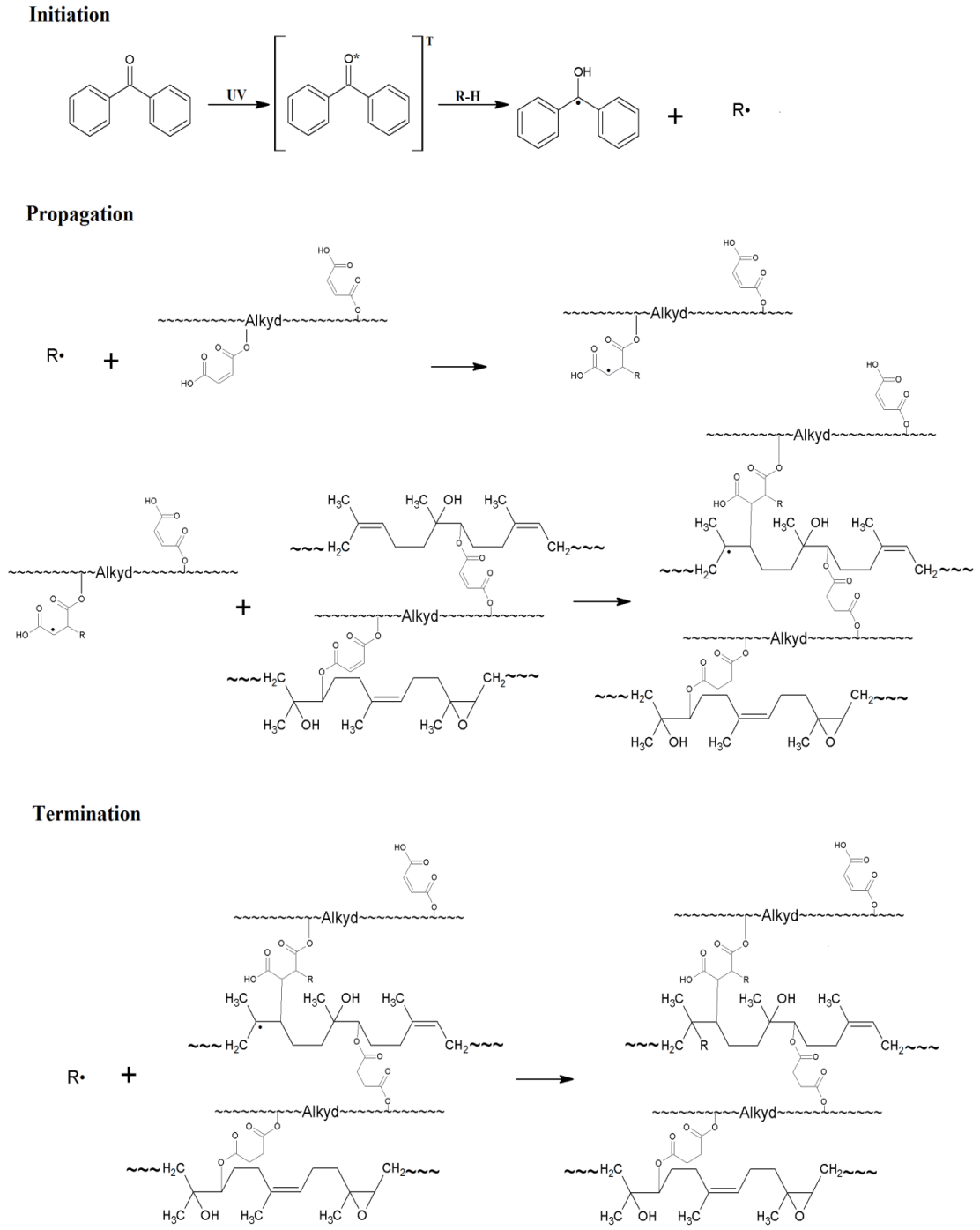

Figure 4.33: Proposed reactions that took place during UV irradiation of ENR50/AlkydMA1 blend

4.7.2 Swelling percentage and crosslink density

Swelling percentage of the gel obtained after immersion of EA-B0T0 and EA-B5T0 blends in toluene for 48 hours is shown in Figure 4.34. Initially, % of swelling of the toluene insoluble fraction obtained from both the blends are rather high where EA-B0T0 blend recorded 3569 % of swelling while EA-B5T0 blend swells about 4367 %. However, upon UV irradiation, swelling % of the gel obtained from EA-B5T0 blend decreased significantly. Presence of benzophenone in the blend has initiated crosslinking involving the C=C group in the system and produced a network that could resist penetration of solvent into the gel.

EA-B0T0 blend also shows a decreasing trend in its swelling % when the UV irradiation time was prolonged from 0 s to 240 s. Swelling % of the gel drops by a total of 1963 % to 1606 % after the blend was irradiated with UV light for 240 s. This further supports that the blend film could had undergone some extent of crosslinking during UV irradiation leading to the increase in its gel content.

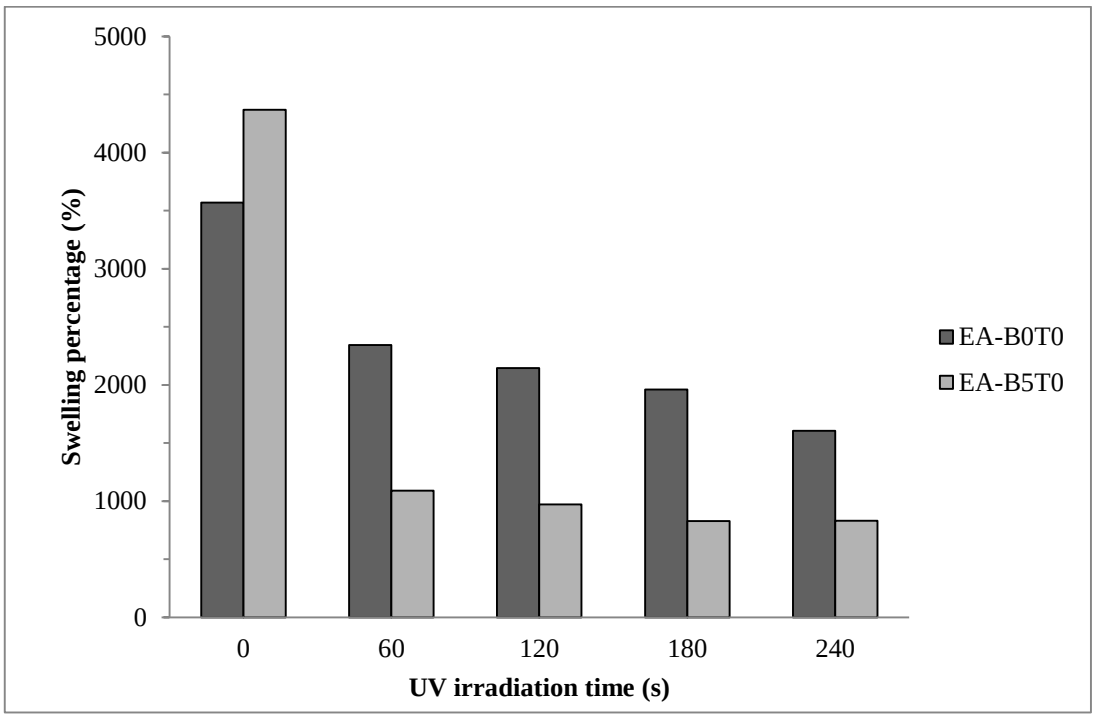

Figure 4.34: Variation of swelling % in EA-B0T0 and EA-B5T0 blends at different UV irradiation time

Data obtained from the swelling of the crosslinked polymers in toluene are fitted to the Flory-Rehner equation to calculate the average molecular weight between crosslinks, M_c and crosslink density, υ of the UV-cured EA-B0T0 and EA-B5T0 blends. The results are shown in Table 4.14 and 4.15 respectively. As expected, M_c of the blends follow the same trend as the swelling percentage where the values decrease when the blending time is prolonged. Higher crosslink density value was observed in blend which incorporated with benzophenone and subjected to longer UV-curing time.

Table 4.14: Percentage of swelling in toluene, crosslink density and average molecular weight between crosslink of UV-cured EA-B0T0 blends

Parameters	UV irradiation time (s)				
	0	60	120	180	240
Swelling %	3569	2343	2146	1962	1606
Density of blend, ρ (g cm^{-3})	0.973	0.973	0.973	0.973	0.973
Density of solvent, ρ_1 (g cm^{-3})	0.867	0.867	0.867	0.867	0.867
Volume fraction of polymer in the swollen gel, ϕ	0.024	0.037	0.040	0.043	0.053
Solvent-polymer interaction parameter, χ	0.351	0.351	0.351	0.351	0.351
Crosslink density, v (x 10^{-6} mol cm^{-3})	3.14	6.46	7.51	8.77	12.4
Average molecular weight between crosslink, M_c (x 10^5 g mol^{-1})	3.10	1.51	1.29	1.11	0.79

Table 4.15: Percentage of swelling in toluene, crosslink density and average molecular weight between crosslink of UV-cured EA-B5T0 blends

Parameters	UV irradiation time (s)				
	0	60	120	180	240
Swelling %	4367	1090	971	828	833
Density of blend, ρ (g cm^{-3})	0.968	0.968	0.968	0.968	0.968
Density of solvent, ρ_1 (g cm^{-3})	0.867	0.867	0.867	0.867	0.867
Volume fraction of polymer in the swollen gel, ϕ	0.020	0.076	0.084	0.098	0.097
Solvent-polymer interaction parameter, χ	0.351	0.351	0.351	0.351	0.351
Crosslink density, v (x 10^{-5} mol cm^{-3})	0.22	2.46	3.01	3.97	3.94
Average molecular weight between crosslink, M_c (x 10^4 g mol^{-1})	43.2	3.94	3.22	2.44	2.46

4.7.3 DSC analysis

DSC analyses were carried out to determine T_g of the blends after they were irradiated with UV light for different duration of time. As shown in Figure 4.35, T_g of EA-B0T0 blends remain constant at approximately -21.0 °C, before and after UV irradiation. However, the additional 5 phr of benzophenone in EA-B5T0 blend has resulted in a rather big increase in the T_g of the blend after they were irradiated with UV light, shown in Figure 4.36. The benzophenone in the blend was responsible to generate radical to propagate crosslinking involving unsaturation sites in the blend. That explains the increase in the T_g of the blend from -23.5 °C to -17.2 °C after 240 s of UV irradiation. Interestingly, T_g of the control blend (EA-B0T0) was higher than the blend containing benzophenone (EA-B5T0) prior to UV irradiation. Presumably, presence of small molecules such as benzophenone in the blend could have disturbed the chain packing in the system, and consequently lowers the T_g.

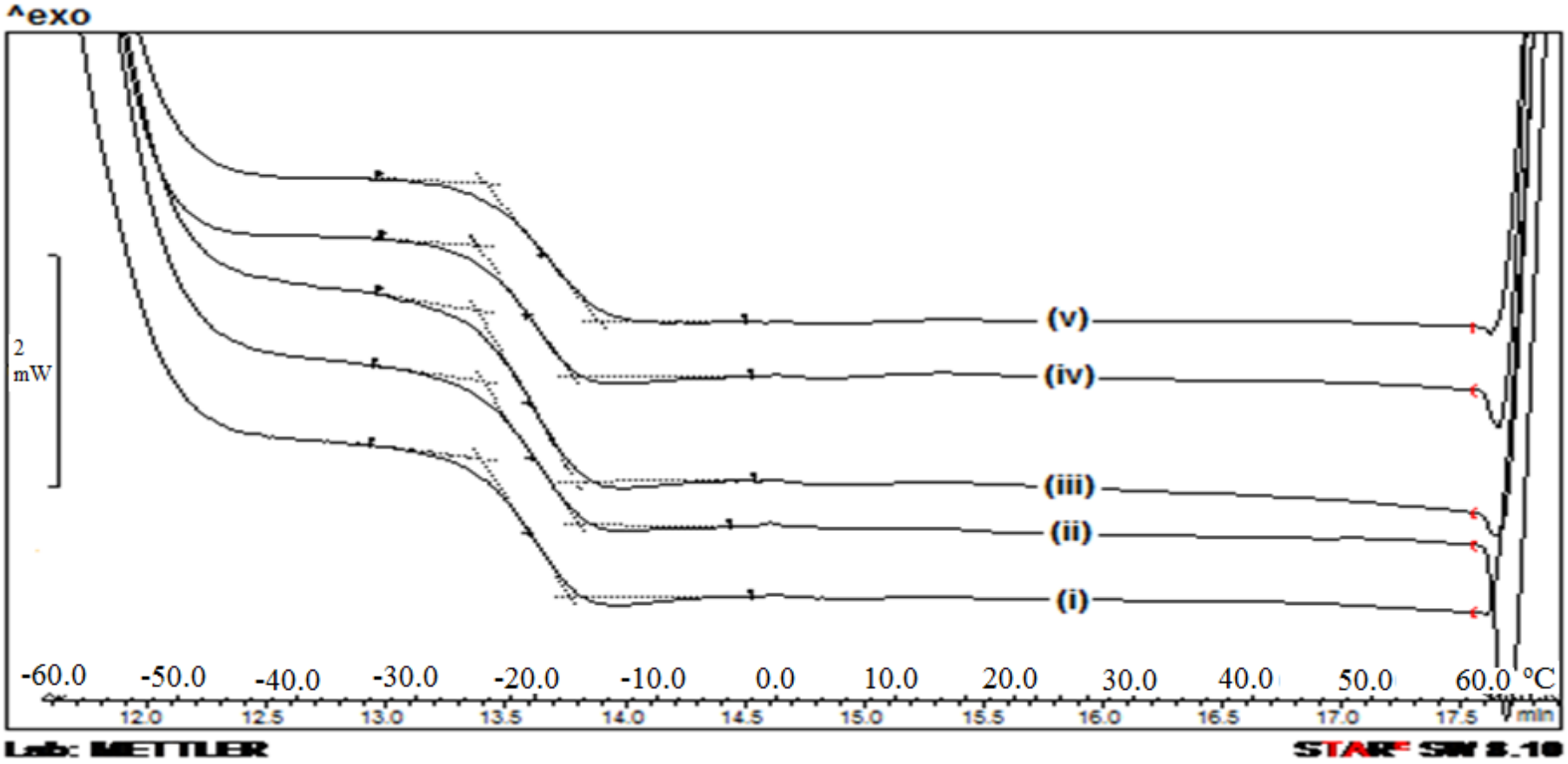

Figure 4.35: DSC thermograms of EA-B0T0 blends after irradiated with UV light for different duration of time: (i) 0 s, (ii) 60 s, (iii) 120 s, (iv) 180 s, and (v) 240 s.

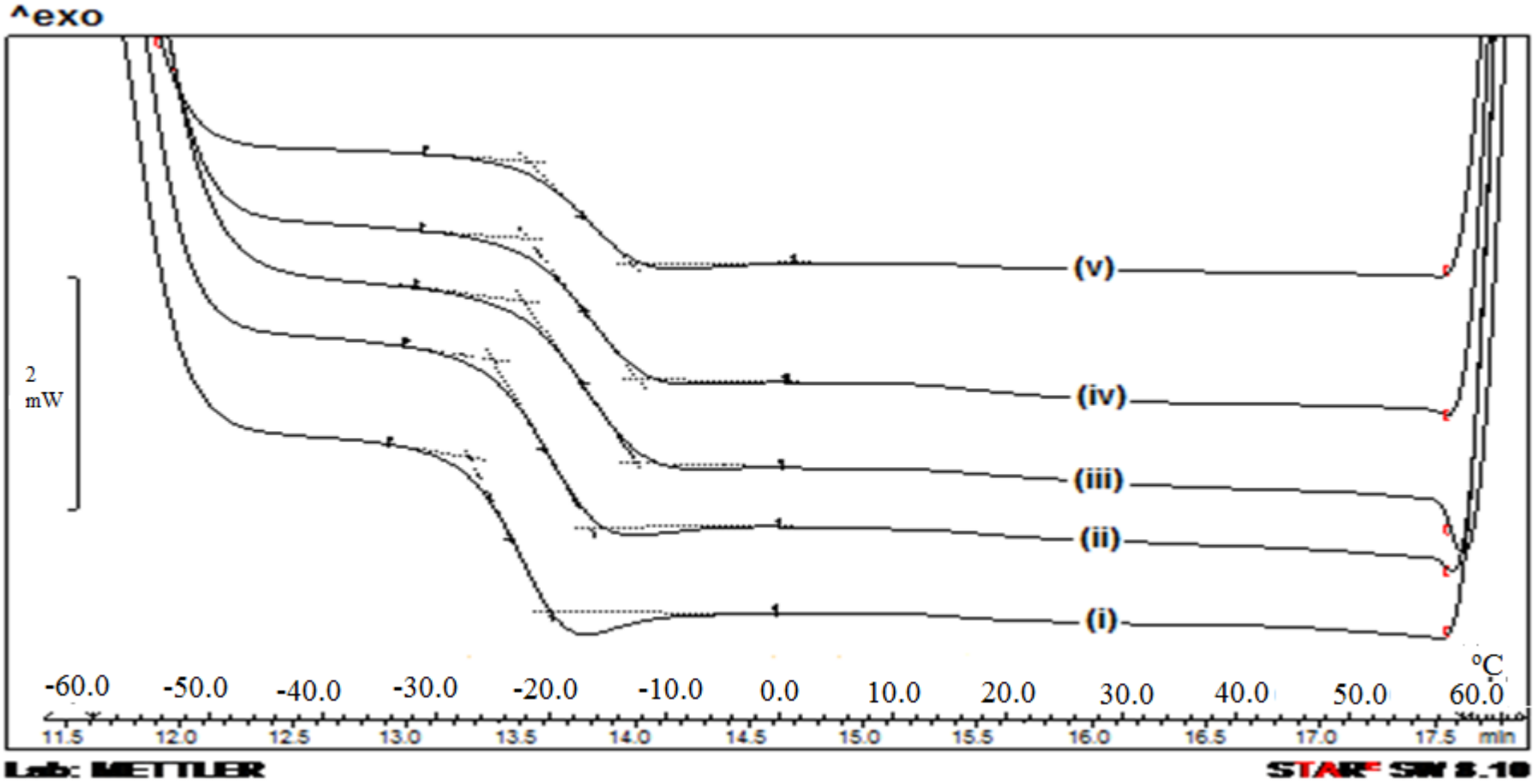

Figure 4.36: DSC thermograms of EA-B5T0 blends after irradiated with UV light for different duration of time: (i) 0 s, (ii) 60 s, (iii) 120 s, (iv) 180 s, and (v) 240 s.

4.8 Enhancing UV-induced crosslinking in ENR50/AlkydMA1 blend via incorporation of TMPTA

4.8.1 Gel fraction

The effect of adding TMPTA on the extent of radiation-induced crosslinking of the blends can be estimated from the gel fractions obtained after immersion in toluene. Figure 4.37 shows the percentage of gel obtained in EA-B5T0, EA-B5T1, EA-B5T3 and EA-B5T5 blends as a function of UV irradiation time. As seen in the plot, addition of TMPTA into the blends has resulted in significant increase in the amount of gel obtained upon irradiation. It should be reminded that individual components in the blend are easily soluble in toluene. However, upon blending and subsequent UV irradiation, the products are able to resist total dissolution in toluene. In fact, blend formulated with higher amount of TMPTA (5 phr of TMPTA) produced as high as > 90 % of gel. This is not totally unexpected as TMPTA is well known as a reactive additive which forms crosslink bridges via irradiation-induced free radical mechanism.

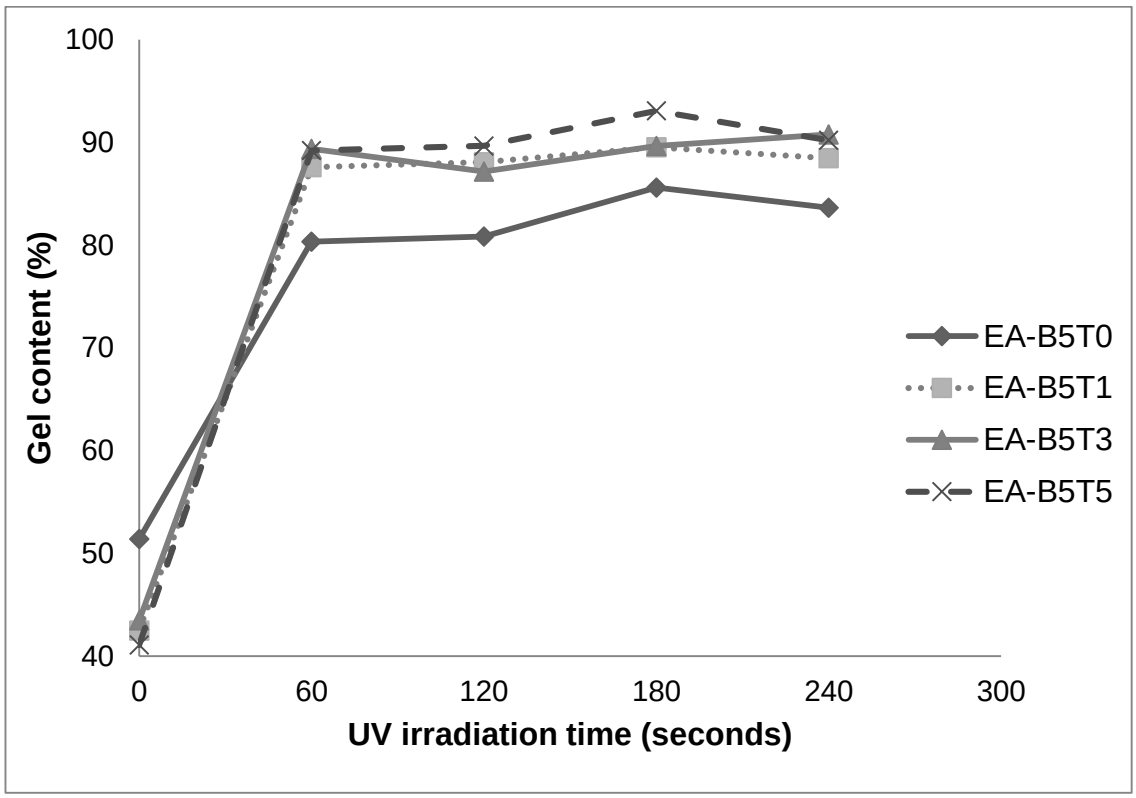

Figure 4.37: Effect of adding TMPTA on the gel content of UV-induced crosslinking in ENR50/AlkydMA1 blends

Table 4.16-4.18 summarise the swelling test results, together with the calculated crosslink density, *v* and average molecular weight between crosslinks, M_c of the UV-cured EA-B5T1, EA-B5T3 and EA-B5T5 blends respectively. Comparing the % swelling of EA-B5T1 blend, irradiated with UV light for 240 s (Table 4.16) with those of EA-B5T0 blend (Table 4.15), presence of 1 phr of TMPTA in the blend manage to reduce the % swelling by almost half. Therefore, regardless of the actual mechanism of radiation-induced reactions involved, the results prove the important role played by TMPTA in enhancing the radiation-induced crosslinking in the UV-cured ENR50/AlkydMA1 blend. % swelling in the blends containing TMPTA was also observed to decrease with the increasing amount of TMPTA incorporated. The increase in crosslink density in the UV-cured blend could resist the expansion of the polymer networks during the immersion, thus preventing it from accommodating excessive

solvent. The molecular weight between crosslinks has also reduced due to the increase in the crosslink density.

Table 4.16: Percentage of swelling in toluene, crosslink density and average molecular weight between crosslink of UV-cured EA-B5T1 blends

Parameters	UV irradiation time (s)				
	0	60	120	180	240
Swelling %	4337	610	520	465	449
Density of blend, ρ (g cm^{-3})	0.994	0.994	0.994	0.994	0.994
Density of solvent, ρ_1 (g cm^{-3})	0.867	0.867	0.867	0.867	0.867
Volume fraction of polymer in the swollen gel, ϕ	0.020	0.125	0.144	0.158	0.163
Solvent-polymer interaction parameter, χ	0.351	0.351	0.351	0.351	0.351
Crosslink density, v (x 10^{-5} mol cm^{-3})	0.22	6.51	8.64	10.5	11.2
Average molecular weight between crosslink, M_c (x 10^4 g mol^{-1})	45.8	1.53	1.15	0.95	0.89

Table 4.17: Percentage of swelling in toluene, crosslink density and average molecular weight between crosslink of UV-cured EA-B5T3 blends

Parameters	UV irradiation time (s)				
	0	60	120	180	240
Swelling %	3995	531	437	401	330
Density of blend, ρ (g cm^{-3})	0.999	0.999	0.999	0.999	0.999
Density of solvent, ρ_1 (g cm^{-3})	0.867	0.867	0.867	0.867	0.867
Volume fraction of polymer in the swollen gel, ϕ	0.021	0.140	0.166	0.178	0.208
Solvent-polymer interaction parameter, χ	0.351	0.351	0.351	0.351	0.351
Crosslink density, v (x 10^{-5} mol cm^{-3})	0.25	8.24	11.7	13.6	19.1
Average molecular weight between crosslink, M_c (x 10^4 g mol^{-1})	40.4	1.21	0.86	0.74	0.52

Table 4.18: Percentage of swelling in toluene, crosslink density and average molecular weight between crosslink of UV-cured EA-B5T5 blends

Parameters	UV irradiation time (s)				
	0	60	120	180	240
Swelling %	3513	368	350	320	318
Density of blend, ρ (g cm^{-3})	1.024	1.024	1.024	1.024	1.024
Density of solvent, ρ_1 (g cm^{-3})	0.867	0.867	0.867	0.867	0.867
Volume fraction of polymer in the swollen gel, ϕ	0.023	0.187	0.195	0.209	0.210
Solvent-polymer interaction parameter, χ	0.351	0.351	0.351	0.351	0.351
Crosslink density, v (x 10^{-5} mol cm^{-3})	0.30	15.2	16.6	19.4	19.6
Average molecular weight between crosslink, M_c (x 10^4 g mol^{-1})	34.6	0.68	0.62	0.53	0.52

4.8.2 Thermal analysis

TGA thermograms of UV-cured blends, composing 1-5 phr of TMPTA in their formulations are shown in Figure 4.38, along with those of EA-B5T0 blend. T_i, which is the temperature at which 1 % of weight loss has taken place is used to compare the thermal stability of the sample, before (0 s) and after (240 s) UV-curing. Results from TGA analysis show that there is an increment in T_i for each blend after they were irradiated with UV light, indicating improvement in the tolerance of the blends towards thermal degradation as a results of the formation of irradiation-induced crosslink. Besides, blends that were formulated with TMPTA as crosslinker experienced higher shift in their T_i, especially in EA-B5T5 blends, where T_i of the blend increased from 191.1 °C to 234.1 °C after UV irradiation. This is a clear evidence to support the

presence of greater amount of crosslinked structure in the blend as a result of the introduction of trifunctional monomer.

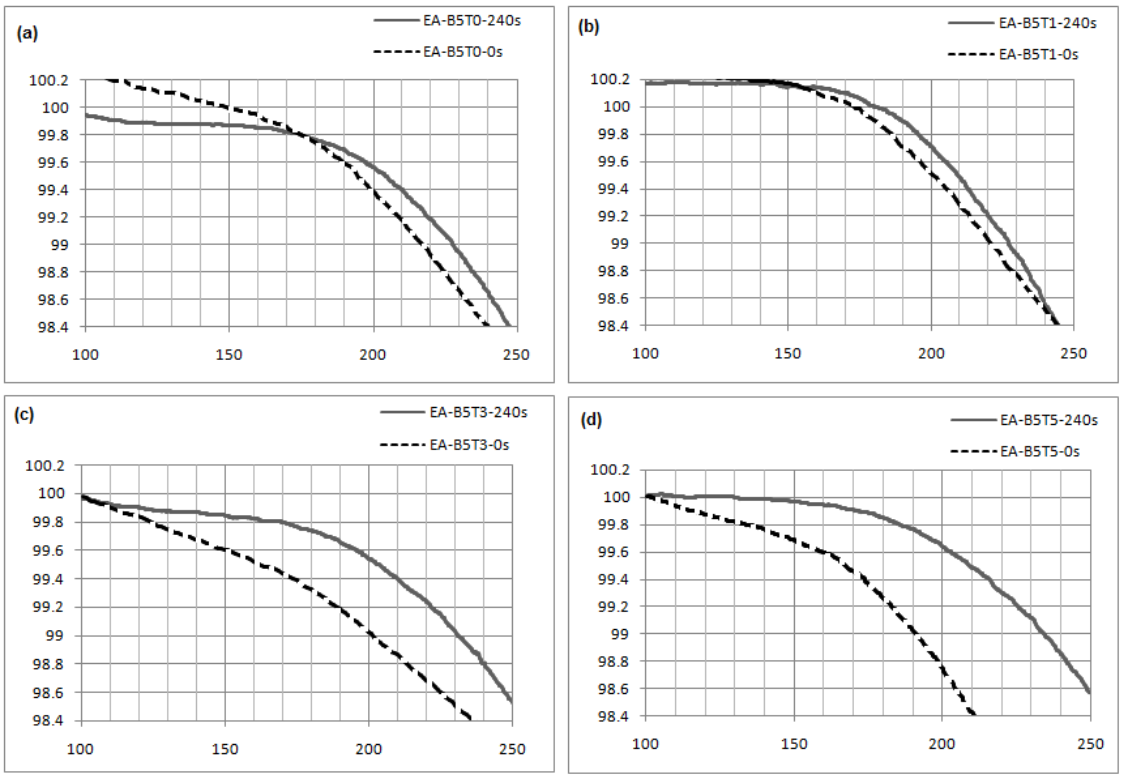

Figure 4.38: TGA thermograms of (a) EA-B5T0 blend, (b) EA-B5T1 blend, (c) EA-B5T3 blend, and (d) EA-B5T5 blend

The UV-cured blends incorporated with TMPTA were also analysed by DSC and their thermograms are shown in Figure 4.39-4.41. Comparing T_g values of the blends with those of EA-B5T0 blend series, incorporation of TMPTA as crosslinker has helped to further elevate the T_g. While EA-B5T0 blends recorded a positive shift by 6 °C in T_g values after 240 s of UV irradiation, introduction of 0.01 weight % of TMPTA was sufficient to increase the T_g of EA-B5T1 blends from -23.1 °C to -16.6 °C under the same exposure UV light. It is not surprising, as each TMPTA molecule contain 3 unsaturation sites which participate in irradiation-induced crosslinking in the blend, hence reduces the degree of freedom in the polymer chains. The same increasing trend

in T_g were observed in the other two blend series, with higher amount of TMPTA loading (EA-B5T3 and EA-B5T5). However, T_g of the blends did not elevate further than -16.6 °C but remain constant at that temperature after certain duration of UV irradiation. As seen in Figure 4.40, T_g of uncured EA-B5T3 blend is -22.1 °C, which later increased to -17.3 °C after 120 s of UV irradiation. Beyond 180 s of UV irradiation, T_g of the blends started to be constant at -16.5 °C. T_g of EA-B5T5 blend (Figure 4.41) however started to remain constant at -16.6 °C after 120 s of UV irradiation time.

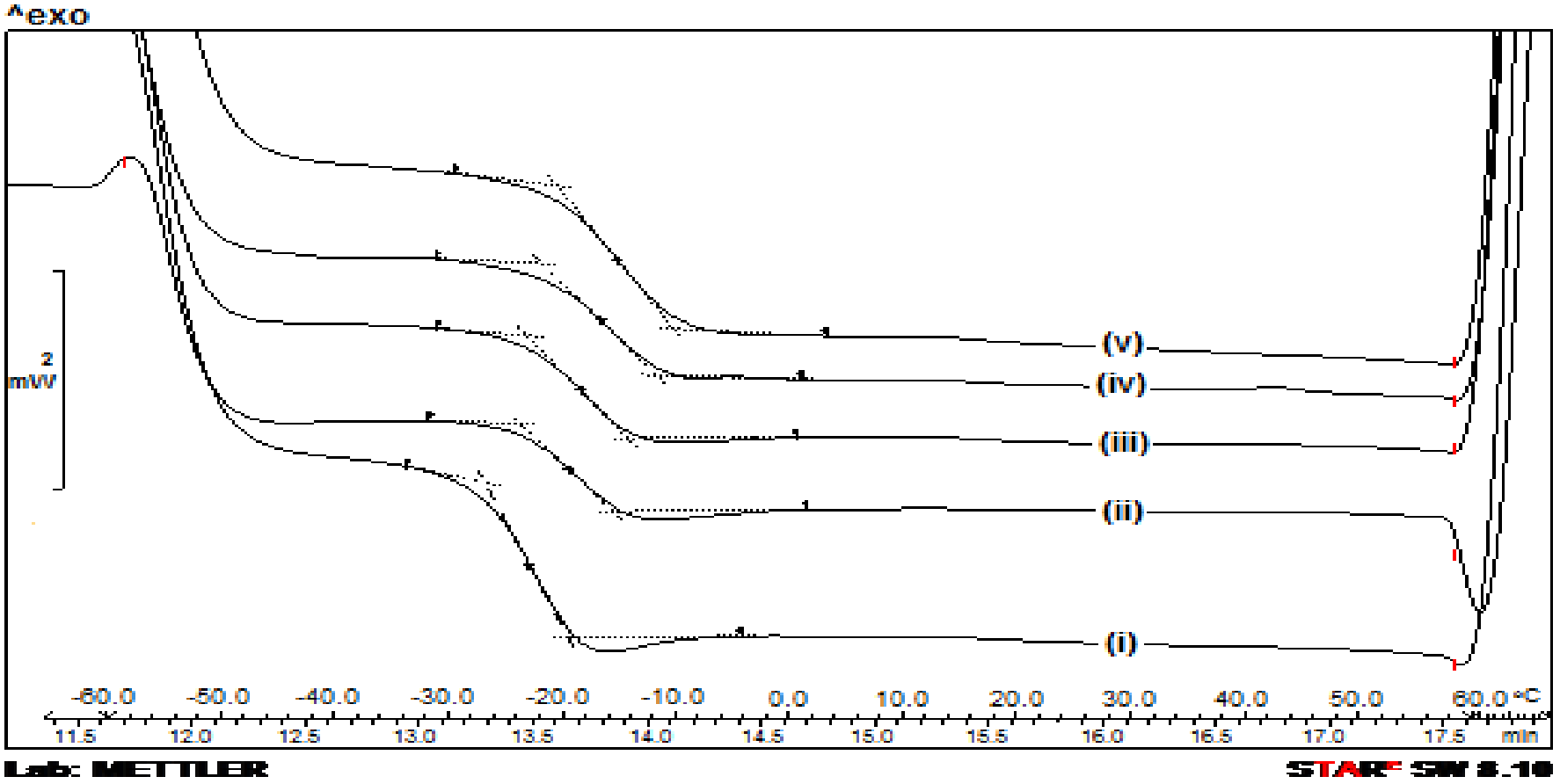

Figure 4.39: DSC thermograms of EA-B5T1 blends after irradiated with UV light for different duration of time: (i) 0 s, (ii) 60 s, (iii) 120 s, (iv) 180 s, and (v) 240 s

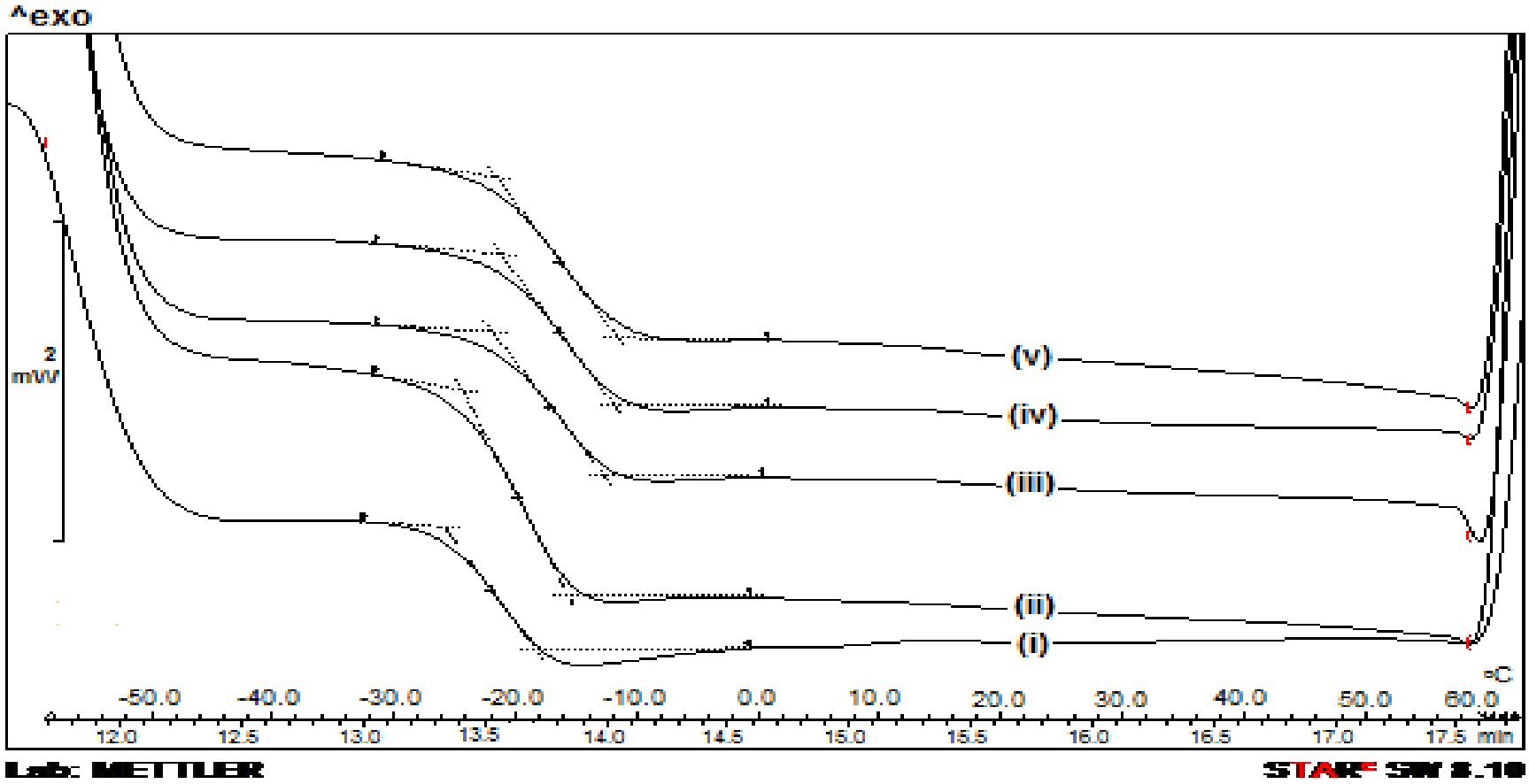

Figure 4.40: DSC thermograms of EA-B5T3 blends after irradiated with UV light for different duration of time: (i) 0 s, (ii) 60 s, (iii) 120 s, (iv) 180 s, and (v) 240 s

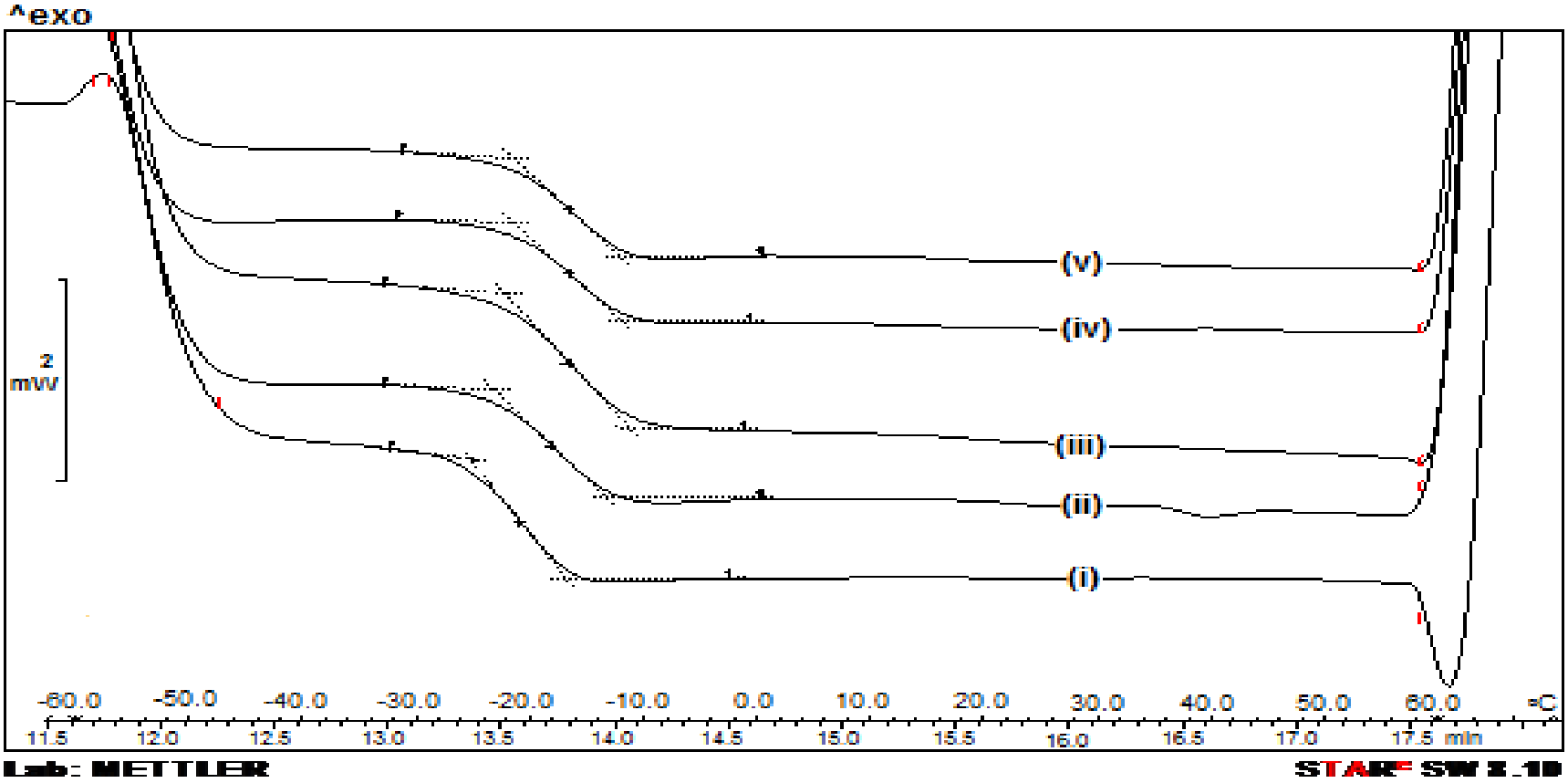

Figure 4.41: DSC thermograms of EA-B5T5 blends after irradiated with UV light for different duration of time: (i) 0 s, (ii) 60 s, (iii) 120 s, (iv) 180 s, and (v) 240 s.

4.8.3 FTIR analysis

Thin films from EA-B5T3 blend series, obtained after UV-curing for different intervals of time were analysed by FTIR to study the changes in the spectrum during curing process. Figure 4.42(a) shows the normalised FTIR spectra of EA-B5T3 blend series after irradiated with UV light for different intervals of time. All the peaks in the spectra were normalised against an internal standard peak at 1448 cm^{-1} to overcome the effect of uneven sample thickness during FTIR analysis. As seen in the spectra, the peak absorbance at 838 cm^{-1} which corresponds to the =C-H out of plane deformation of the isoprene unit from ENR50 has progressively decreased with UV irradiation. The plot of changes in the peak absorbance ratio of A_{838}/A_{1448} for EA-B5T3 blend series with UV irradiation time is presented in Figure 4.42(b). The reduction in the peak intensity suggests that crosslinking reaction involving -CH=C(CH_3)- of ENR50 has taken place during UV irradiation. This may be either between the unsaturation sites from different ENR50 chain, or presumably due to the bond formation between an isoprene unit with the -CH=CH- from TMPTA and grafted MA in the alkyd chain. The plausible structure of UV-cured EA-B5T3 blend is proposed in Figure 4.43 (Khong et al., 2014).

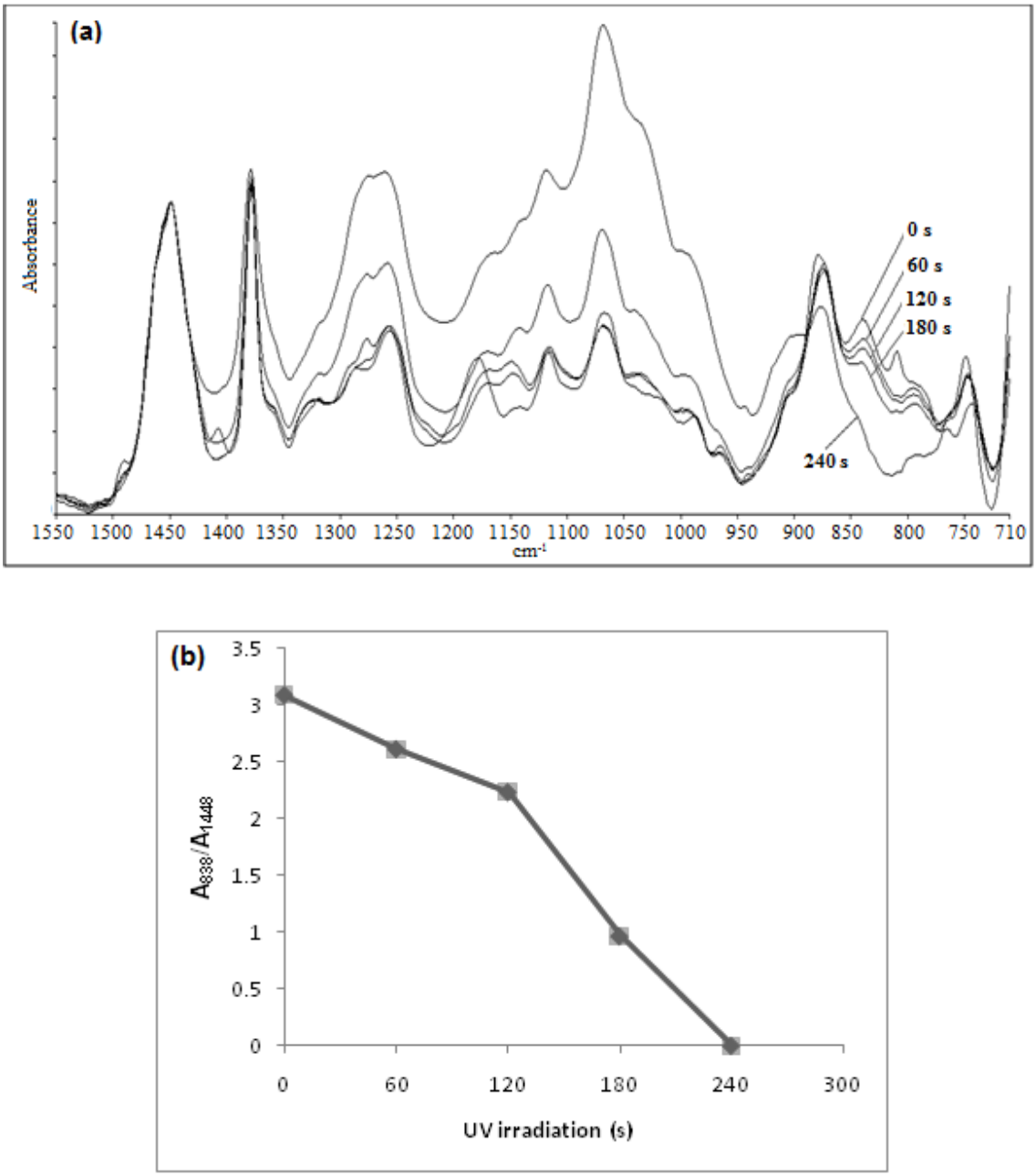

Figure 4.42: (a) Normalised FTIR spectra, and (b) Plot of peak absorbance A_{838}/A_{1448} of EA-B5T3 blend series after irradiated with UV light for different intervals of time

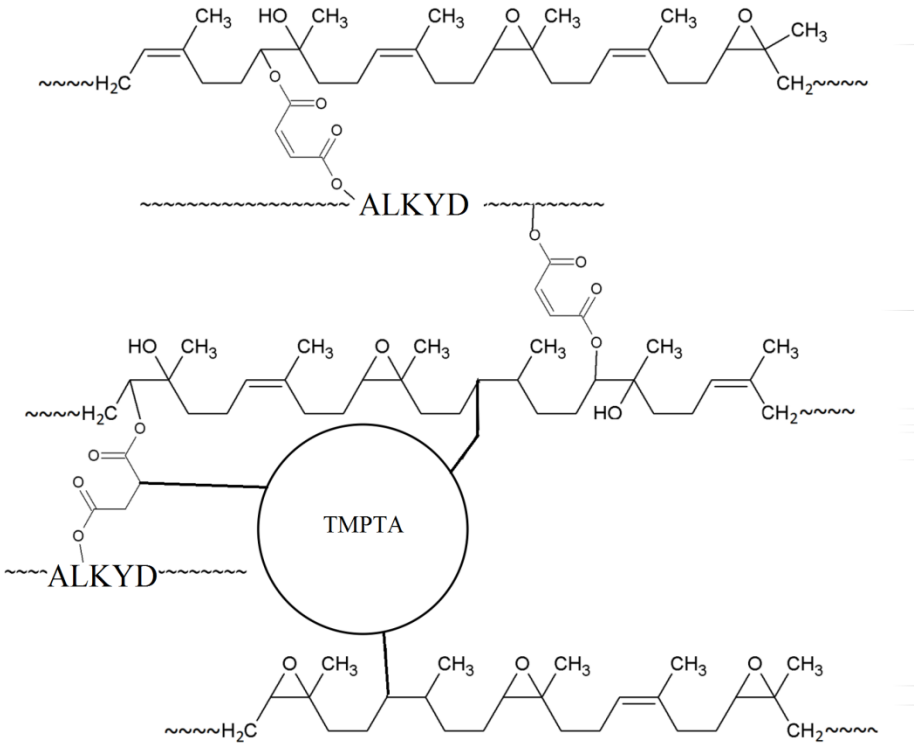

Figure 4.43: Proposed structure of UV-cured EA-B5T3 blend